Synthesis, thermal, structural and linear optical properties of new glasses within the TeO2-TiO2-WO3 system

Mohammed Reda Zaki, David Hamani, Maggy Colas, Jean-René Duclere, Olivier Masson, Philippe Thomas

Synthesis, thermal, structural and linear optical properties of new glasses within the TeO_2-TiO_2-WO_3 system

Mohammed Reda ZAKI, David HAMANI*, Maggy DUTREILH-COLAS, Jean-René DUCLÈRE, Olivier MASSON and Philippe THOMAS

Laboratoire Science des Procédés Céramiques et de Traitements de Surface (SPCTS) – UMR 7315 CNRS, Université de Limoges, Centre Européen de la Céramique, 12 rue Atlantis, 87068 Limoges Cedex, FRANCE

* Corresponding author: David HAMANI, E-mail: david.hamani@unilim.fr

Abstract.

The glass-forming domain and physical properties, namely, the density, thermal, structural and linear optical properties of new glasses within the TeO_2-TiO_2-WO_3 system have been investigated. By means of micro-Raman spectroscopy, the structure of these glasses was examined based on a full-scale spectral decomposition. The optical transmission and refractive index dispersion were measured by UV-Vis-NIR spectroscopy and spectroscopic ellipsometry respectively. Consistent correlations were established between the structural and linear optical properties. Only minor structural modifications of the original TeO_2-rich network are taking place upon adding TiO_2 or WO_3, suggesting the absence of Te–O–Te bond network depolymerization. Our results also suggest that, upon increasing TiO_2 content, a phase separation occurs between amorphous TeO_2-rich and amorphous TiO_2-rich regions. We also argue that the structural trends upon adding WO_3 evolve from uniformly dispersed WO_6 octahedra (at low WO_3 content) to amorphous WO_3-like regions (at higher WO_3 content) before the crystallization of γ-WO_3 at 30 mol.% of WO_3. The compositional dependence of the refractive index and several optical constants (Urbach E_U and dispersion E_d energies, oxide ion polarizabilities) is highlighted. These glasses collectively exhibit high refractive indices in the order of ~2.2.

Graphical abstract.

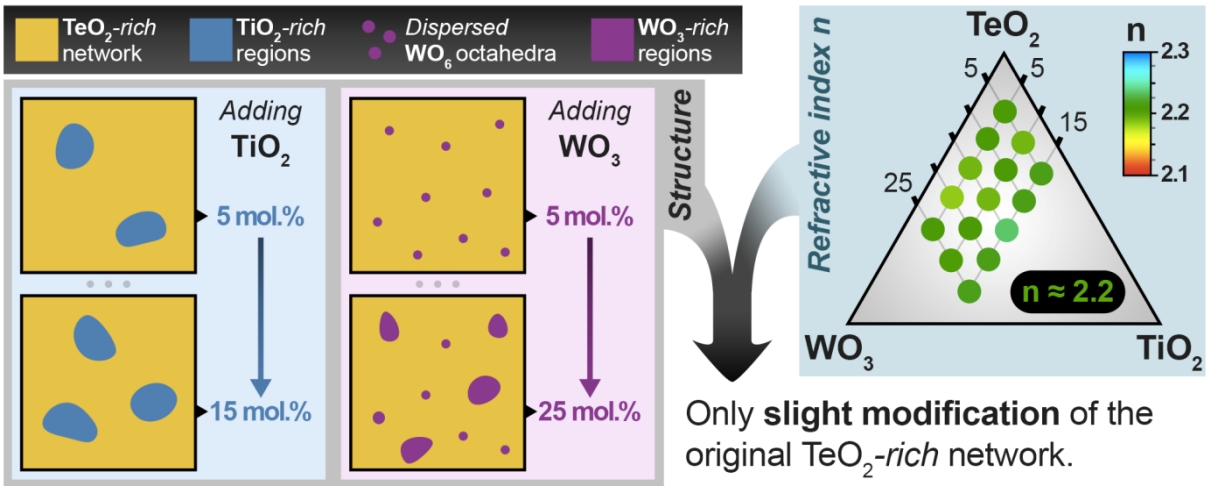

Highlights.

- New glass-forming domain within the TeO_2-TiO_2-WO_3 system was determined.
- Relevant correlations between the structural and optical properties are established.
- Structural effects of TiO_2 and WO_3 are revealed and discussed in detail.
- The investigated glasses exhibit high refractive indices in the order of ~2.2.

Keywords.

Tellurite glasses; glass structure; Raman spectroscopy; linear optical properties.

1. Introduction.

In the past two decades, tellurium oxide-based glasses have attracted a great deal of interest owing to their potential applications as fiber amplifiers and nonlinear optical devices [1–3]. They are still regarded as considerably promising optical materials thanks to, *inter alia*, remarkable optical properties, good thermal and chemical stabilities, and low glass transition temperatures [3]. The understanding of the origins behind the above set of physical properties is an ongoing subject matter in glass science. Therefore, a great deal of attention is still being devoted to establish the physical properties–structure relationships in these TeO_2-based glasses.

Routinely, the structural description of TeO_2-rich glasses is closely influenced by the study of the parent crystalline phases and pure TeO_2 glass. Similarities between the pure TeO_2 glass and the γ-TeO_2 crystal structures were highlighted [4,5]. The latter is composed of *(i)* TeO_4, or more precisely TeO_{3+1} distorted disphenoids with one Te–O bond longer (2.197 Å) than the other three ones (1.859, 1.948 and 2.019 Å) and the presence of a lone electron pair for each Te^{4+} cation constraining the short- and medium-range structure; *(ii)* asymmetric Te–O–Te bridges (1.859–2.197 Å) and nearly symmetric ones (1.948–2.019 Å). By comparing the γ-TeO_2 compound and pure TeO_2 glass using Raman spectroscopy (*cf.* Fig. 3 in [4]), it has been argued that such nearly symmetric bridges constitute one of the main structural features of the TeO_2 glass. Representing the near-medium-range structure, these bridges are responsible for the broad Raman band in the 400-550 cm^{-1} region.

From the optical properties viewpoint, the high linear and nonlinear optical indices of TeO_2-based glasses have been associated with the presence of the Te^{4+} lone electron pair [6–10] and characteristic Te–O–Te bridges [3,11–13]. It has been shown that this inherently high optical response can be further improved upon adding transition metal oxides of empty d-orbital

cations, such as titanium oxide TiO_2 or tungsten oxide WO_3 [14,15]. Moreover, it is well established that adding modifier oxides to TeO_2 glass induces the structural transformation of TeO_4 disphenoids into TeO_3 trigonal pyramids, and therefore contributes to the short-range modification of the glass network [3,16,17]. This transformation is regarded as a "structural depolymerization" since it reduces the network crosslinking density by breaking Te–O–Te bridges. Moreover, it has been demonstrated that this transformation is accompanied with a decrease of the nonlinear optical properties [3,18]. By means of Raman spectroscopy, some authors claimed that adding WO_3 induces this structural depolymerization in TeO_2-based glasses [19,20], which is not the case upon adding TiO_2 [21–23].

Adding TiO_2 to TeO_2 allows to *(i)* enhance the glass-forming ability and obtain homogeneous glasses in the (100-x)TeO_2-xTiO_2 binary system with a glass-forming domain up to x = 18 mol.%, and *(ii)* maintain the original structural organization of pure TeO_2 glass [22,24]. Hence, TiO_2-containing TeO_2-based glasses are of special interest thanks to the positive role of TiO_2 in conserving the glass network of pure TeO_2 which contributes to the high linear and nonlinear optical properties [15,18,23,25]. Most of the preceding studies [21,24,25] dealing with the structure of TeO_2-TiO_2 glasses supported the existence of Te–O–Ti bridges replacing the Te–O–Te ones in the glass network upon increasing TiO_2 content. This idea is based on the unique phase from the TeO_2-TiO_2 system, $TiTe_3O_8$ [26], which features interconnected TeO_4 and TiO_6 polyhedra via nearly symmetric Te–O–Ti bridges with the following bond lengths: 1.867 Å and 1.955 Å respectively.

With increasing WO_3 content in binary TeO_2-WO_3 glasses, the thermal and optical properties are progressively improved [15,27]. These glasses have been extensively studied and the fact that no crystalline phase, *i.e.* no "parent crystalline model", has ever been identified in the binary TeO_2-WO_3 system led to considerable efforts for the understanding of their structural features. Most of these studies focused on the tungsten local environment (to demonstrate

whether WO_4 or WO_6 polyhedra exist in the glass network) using IR and/or Raman spectroscopy techniques [28–31]; yet, despite many efforts, this basic information is still obscure and controversial [19,32–35]. In this paper, we will bring to light the local structure around W^{6+} cations in WO_3-containing TeO_2-based glasses. It was shown from previous works using Raman spectroscopy [29,30,32] that compared with the Raman spectrum of TeO_2 glass, three additional major bands (at ~360, 860 and 925 cm^{-1}) appear at the Raman spectra of WO_3-containing TeO_2-based glasses and their intensities increase upon adding WO_3. It is generally agreed that the high-wavenumber band at 925 cm^{-1} originates from the stretching mode of the shortest W–O bonds. Sekiya *et al.* [29] suggested the growth of clusters of corner-sharing WO_6 octahedra with increasing WO_3 content in TeO_2-WO_3 glasses. It is important to recall here the existence of corner-sharing distorted WO_6 octahedra in the γ-WO_3 compound with twelve distinct W–O bond lengths ranging from 1.714 to 2.159 Å [36].

Keeping the above facts in focus, we have embarked upon studying dual-transition metal oxide-containing TeO_2-based glasses within the (100-x-y)TeO_2-xTiO_2-yWO_3 ternary system (labeled TTxWy). To the best of our knowledge, only a handful studies have investigated compositions within the TeO_2-TiO_2-WO_3 system. First, Safonov [37] attempted to determine its equilibrium and non-equilibrium phase diagram; Muñoz-Martín *et al.* [38] prepared and measured the structural and optical properties of the glass composition 80TeO_2-5TiO_2-15WO_3; and finally, a similar investigation was performed by Fares *et al*. [20] on the following *quaternary composition*: (89-x)TeO_2-10TiO_2-xWO_3-1Nd_2O_3.

The aim of the present paper is to report the glass-forming domain within the TTxWy system, the glasses' thermal characteristics, their structural features as probed by micro-Raman spectroscopy and finally, their linear optical properties from the optical transmission and spectroscopic ellipsometry measurements. The focus is laid on the evolution of these properties as a function of TiO_2 and WO_3 contents.

2. Experimental details.

New glasses were prepared within the ternary TTxWy system by the conventional melting-quenching technique using α-TeO_2 (99.99%) and WO_3 (99.8%) both from Alfa Aesar, and anatase TiO_2 (99+%) from Sigma-Aldrich. In appropriate proportions, the raw dried powders have been ground for 40 minutes using agate mortar and pestle, and melted in Pt crucibles at 850 °C for 1h in air atmosphere. Under these experimental conditions, fifteen glass samples in the form of pellets were prepared from batches weighing 2 g, stirred three times during melting (once every 15 minutes, in order to increase their homogeneity) and quenched from 850 °C into a brass ring put over a preheated brass block at 150 °C. After cooling down from 150 °C, glass pellets were systematically annealed at 15 °C below the glass transition temperature (T_g) for 12 h at a rate of 2 °C/min (during both heating and cooling) in order to release the mechanical stresses resulting from fast thermal quenching.

Moreover, to properly interpret the structural properties of TTxWy glasses, we have prepared pure TeO_2 and binary (100-x)TeO_2-xTiO_2 glasses (labeled TTx) by fast-quenching the melts from 850 °C down to approximately -11 °C (using an ice bath containing NaCl and ethanol) after 1 hour spent inside the furnace during which the melts were stirred three times.

To check the amorphous state of the samples, X-ray diffraction patterns were recorded from powder samples using Bruker D8 Advance diffractometer with Bragg-Brentano geometry (copper $K_{\alpha 1}$ wavelength of 1.5406 Å, angular 2θ range of 10-70° with a step of 0.02° and 1s per step). The glass samples were analyzed by energy dispersive X-ray microanalysis (EDS) using a Quanta FEG-450 scanning electron microscope. The elemental analysis results showed that the experimental glass compositions were in good agreement with the theoretical ones. The characteristic temperatures of glasses, namely the glass transition (T_g) and onset

crystallization (T_O) temperatures were measured by heat flux differential scanning calorimetry (DSC) using NETZSCH STA 449 F3 Jupiter equipment. About 25 ± 5 mg of glass fragments were put into Pt pans, and the measurements were performed under N_2 atmosphere between room temperature and 720 °C at a heating rate of 10 °C/min. Densities of glass powder samples (150 ± 20 mg) were measured by helium pycnometry using Accupyc II 1340 pycnometer from Micromeritics.

The Raman spectra of the obtained glass samples were recorded at 514 nm using T64000 Horiba Jobin-Yvon spectrophotometer operating in triple subtractive configuration (1800 gr/mm) associated to a liquid nitrogen-cooled CCD detector. The Raman spectra were recorded in the 15-1100 cm^{-1} wavenumber range while focusing the laser beam (exposure time of 10 seconds) at a depth of approximately 2 µm from the top surface of the glass pellets. In each glass sample, three Raman spectra have been recorded from three different spots. The excellent agreement within each set of spectra demonstrates high degrees of topological homogeneity within the samples. As a reliable approach to study the compositional dependence of the Raman spectra, no baseline correction treatments were carried out on any of the measured Raman spectra, and the as-recorded intensities of each spectrum were divided by its total area. Using Focus 1.0 program [39], the total-area averaged Raman spectra were decomposed in the entire wavenumber range (15-1100 cm^{-1}) using a log-normal distribution for the boson peak and twelve Gaussian functions for the rest of the wavenumber range. The calculated spectra are considered to match to the experimental ones with chi-square reliability values less than 0.05.

To evaluate the optical transmission of TTxWy glasses, we measured the UV-Vis-NIR spectra from double side polished pellets of 1.44-1.47 mm in thickness over a wide wavelength range from 300 to 3300 nm using the Varian Cary 5000 spectrophotometer. Using the same samples, the refractive index dispersion was recorded by spectroscopic ellipsometry using a

phase-modulated ellipsometer (Horiba Jobin-Yvon UVISEL) with a fixed 60° incidence angle.

3. Results and discussion.

3.1 Glass-forming domain

The amorphous state of TTxWy samples was checked by X-ray powder diffraction in order to determine the glass-forming domain shown in Fig. 1(a). It extends from x = 5 to 15 mol.% in TiO_2 and y = 5 to 25 mol.% in WO_3. In total, fifteen melt compositions have yielded yellowish-transparent glasses that shifted to honey-brown with increasing WO_3 content and remained practically unchanged upon adding TiO_2 (*cf.* Fig. 1(b)).

Crystals of γ-WO_3 compound [36,40] are detected in TTxW30 samples. The corresponding peaks become sharper and more intense upon adding TiO_2, suggesting an increase of the number and/or average size of WO_3 crystallites. At 20 mol.% of TiO_2, crystals of rutile TiO_2 phase are detected in TT20Wy samples without any trace of crystallizing $TiTe_3O_8$ or anatase TiO_2 phases.

3.2 Density and thermal properties

The densities and thermal characteristics of TTxWy glasses are jointly listed in Table 1. Since very close trends of these properties are observed upon adding TiO_2 (or WO_3) at different WO_3 (or TiO_2) contents, we suggest to consider TTxW5 and TT5Wy sets of samples for the sake of simplicity. The density increases with addition of WO_3 by approximately 6% from TT5W5 (5.586 $g.cm^{-3}$) to TT5W25 (5.925 $g.cm^{-3}$). On the other hand, a density decrease by

approximately 2% is recorded upon adding TiO_2 from TT5W5 (5.586 $g.cm^{-3}$) to TT15W5 (5.454 $g.cm^{-3}$). Therefore, the compositional dependence of the density seems to follow the *additive density rule*: densities of raw oxides TiO_2, TeO_2 and WO_3 are respectively 3.90, 6.13 and 7.16 $g.cm^{-3}$. The density evolutions in TTxWy glasses are logically assigned to the higher molar mass of WO_3 (231.8 $g.mol^{-1}$) and lower molar mass of TiO_2 (79.9 $g.mol^{-1}$) than that of TeO_2 (159.6 $g.mol^{-1}$).

The glass transition temperature T_g in TTxWy glasses increases linearly upon adding either TiO_2 or WO_3 ($T_{g(min)}$= 328 °C and $T_{g(max)}$= 426 °C). It increases by ~16% from TT5W5 (328 °C) to TT15W5 (380 °C) and by ~15% from TT5W5 (328 °C) to TT5W25 (376 °C). A step increase by 10 mol.% in TiO_2 induced an overall rise of T_g that is twice more consequential (increase by ~50 °C) than in the case of WO_3 (increase by ~25 °C).

It is worth pointing out that the thermal stabilities ($\Delta T= T_O-T_g$) which reflect the ability of the glass network to resist against devitrification upon heating above T_g, are fairly moderate among TTxWy glasses (ΔT_{min}= 31 °C and ΔT_{max}= 57 °C) (*cf.* Table 1 and Fig. 2). These thermal stabilities might represent a limiting factor for the use of these glasses in the optical fiber technology, for which as an "experimental standard", a minimum value of 100 °C is needed. Adding TiO_2 induces an increase of ΔT from TT5Wy to TT10Wy glasses before a decrease in TT15Wy glass samples. It seems though that ΔT is marginally improved with continuous increase in WO_3 content.

3.3 Structural properties

3.3.1 Structural effect of adding TiO_2

According to Dietzel's cationic field strength theory [41,42], one of the classical structural theories of glass formation, the concept of field strength (FS) represents the interaction of forces between cations and anions during the melt cooling. It is expressed as follows: FS = Z_c/a^2, where Z_c is the charge number of the cation, and *a* is the sum of ionic radii of the cation and anion. In binary oxide melts where the two constituent cations have very close FS values, a slow cooling rate (towards crystallization) is expected to lead to a **solid solution** type of organization in the crystal; whereas faster cooling/quenching rates (towards glass formation) would result in a **phase separation** between the two pure oxide phases. We calculated the FS values while considering O^{2-}, Te^{4+} and Ti^{4+} ions to be two-fold, four-fold and six-fold coordinated respectively and having the following ionic radii: 1.35 Å, 0.66 Å and 0.605 Å [43]. It is very important to highlight that *(i)* the FS values for Te^{4+} (0.990) and Ti^{4+} (1.047) cations are very close, and that *(ii)* the only reported crystal compound from binary TeO_2-TiO_2 system, namely $TiTe_3O_8$ [26], is in fact a solid solution of TiO_2 in TeO_2 with a ratio of 1:3 respectively. Therefore, since the FS theory proves to be valid for the equilibrium TeO_2-TiO_2 system, one would expect that it would successfully predict the structure of binary TTx glasses as well. In other words, a phase separation within the glass network could be predicted and thus resulting in TeO_2-rich and TiO_2-rich regions. The limited experimentally-detected glass forming ability upon adding TiO_2 (maximum of x = 15 mol.% in both TTx and TTxWy glasses) supports this predicted heterogeneous nature of their glass networks.

To elucidate the structural effect of adding TiO_2, we first examine the TTx system before rushing into the more complicated TTxWy system given that: *(i)* identical glass forming ability upon adding TiO_2 (limited to 15 mol.%) is found in TTx and TTxWy systems; *(ii)* the close force constants of Te–O and Ti–O bonds [22] would likely cause strong overlapping of their corresponding bands in the Raman spectra of TiO_2-containing TeO_2-based glasses.

- *Binary (100-x)TeO_2-xTiO_2 glasses (TTx glasses)*

The recorded Raman spectra from TTx glasses are presented in Fig. 3. They show an intensity increase of bands at ~445, ~615 and ~850 cm^{-1} upon adding TiO_2 from 2.5 to 15 mol.%, and an intensity decrease of bands at ~660 and ~730 cm^{-1}. The assignment of these Raman bands, is given in Table 2; particularly, that of Ti–O vibrations is based on the refs [44–46]. Since the bands at ~660 and ~730 cm^{-1} are associated with Te–O vibrations in TeO_4 and TeO_3 units respectively, their decreasing number with addition of TiO_2 suggests that no structural depolymerization takes place in TTx glasses (as opposed to a striking depolymerization observed in TeO_2-Tl_2O glassy system for example [47]). It appears that this decreasing number of TeO_4 and TeO_3 units is compensated by an increasing number of Ti–O–Ti bridges (at ~445 cm^{-1} and ~615 cm^{-1}) and terminal Ti–O bonds (at ~850 cm^{-1}). The presence of Ti–O–Ti and Ti–O linkages in the glass network is supported by the features of the Raman spectrum of nano-rutile TiO_2 (*cf.* inset in Fig. 3). As highlighted in the inset, the shoulder at ~850 cm^{-1} is only detected from the few-nanometer-sized rutile TiO_2 samples (*cf.* spectrum in orange) and absent in the bulk sample (spectrum in black). It is associated with the antisymmetric stretching vibrations of Ti–O bonds from distorted TiO_{6-x} polyhedra at the surface of TiO_2 nanoparticles [44,45]. Therefore, it seems that amorphous "rutile-like" TiO_2-rich regions (of few nanometers) exist separately from the TeO_2-rich network and their number increases with increasing TiO_2 content from 2.5 to 15 mol.% in TTx glasses before an extensive growth takes place via the crystallization of rutile TiO_2 at 20 mol.% detected by X-ray powder diffraction.

A thorough search of the relevant literature yielded only a single and unanimously accepted structural description of the TiO_2-containing TeO_2-based glasses [21,24,25,48,49] (and above all, the binary TeO_2-TiO_2 glasses [21,22,24]). This description is based on the participation of symmetric Te–O–Ti bridges in the glass network by replacing the original Te–O–Te ones. It was largely supported by the fact that these two bridges are chemically indiscernible, thus

explaining the insignificant changes in the Raman spectra upon adding TiO_2. However, as expressed in the following, we provide here a new viewpoint regarding this description.

Let us consider the symmetric Te–O–Ti bridges. The latter exist in the $TiTe_3O_8$ compound, and their symmetric stretching vibrational mode gives rise to the most intense band at ~477 cm^{-1} (*cf.* Fig. 3). If those symmetric Te–O–Ti bridges truly constituted the backbone of the structural network in TTx glasses, then we would have recorded a significant intensity increase at ~477 cm^{-1} upon adding TiO_2, which is clearly not the case when analyzing the spectra of TTx glasses. Therefore, since the number of Te–O–Ti bridges does not increase with addition of TiO_2 and since the vibrational signature of nano-rutile TiO_2 is observed, we propose that the structure of the glass network is made of "rutile-like" TiO_2-rich regions in a TeO_2-rich network as initially predicted using the field strength theory.

- *Ternary (100-x-y)TeO_2-xTiO_2-yWO_3 glasses (TTxWy glasses)*

The Raman spectra of TTxWy glasses upon adding TiO_2 are given in Fig. 4. A similar spectral evolution, *i.e.* intensity increase at ~445, ~615 and ~850 cm^{-1} is observed from TTxWy glasses. Because of two overlapping bands at ~860 and ~925 cm^{-1} due to vibrating W–O bonds, the intensity increase at ~850 cm^{-1} is less noticeable than from TTx glasses. It is important to recall here that, same as in binary TTx, the glass-forming domain in TTxWy is limited to only 15 mol.% of TiO_2. Hence, it seems that the influence of TiO_2 on a network of either pure TeO_2 (TTx system) or WO_3-containing TeO_2 (TTxWy system) is indifferent.

From the above discussion, we argue that a phase separation between amorphous TeO_2-rich and amorphous "rutile-like" TiO_2-rich regions occurs in TiO_2-containing TeO_2-based glasses. This interpretation is shared with a previous study [50] that predicted phase separation in the 75TeO_2-25TiO_2 glass composition.

3.3.2 Structural effect of adding WO_3

The evolving features of the Raman spectra of TTxWy glasses with increasing WO_3 content (Fig. 5) are in agreement with the reported studies on WO_3-containing TeO_2-based glasses by Raman spectroscopy [19,29,35]. These studies have shown that three additional bands (at ~360, ~860 and ~925 cm^{-1}) emerge at the Raman spectra and increase in intensity upon adding WO_3.

Since the same structural evolutions were observed from TT5Wy, TT10Wy and TT15Wy samples, we suggest to focus on the set of TT5Wy for the sake of simplicity (Fig. 6). The assignment of the Raman bands is given in Table 2. The origin of bands E-J (425-772 cm^{-1}) is supported by previous pioneer works on the vibrational and structural properties of the three TeO_2 polymorphs (α [51], β [51] and γ [4]). The rest of the identified Raman bands (C-D extending from 230 to 351 cm^{-1} and K-M from 820 to ~934 cm^{-1}) are associated with the vibrational response of distorted WO_6 octahedra. The basis of the previous assignment is a bilateral analysis of the vibrational (Raman spectra) *vs.* structural features that we conducted on a large number of tungsten-containing oxides (metal tungstates for the most part). A similar approach has been previously undertaken on few tungstates by Sekiya *et al.* [29]. In the low-wavenumber region, the band B is attributed to intra-chain vibrations of Te–Te bonds (as in amorphous metallic trigonal Te [52]) and the band A (boson peak) is linked to the glass network at medium-range scale [53,54].

For the spectral decomposition, we used a conventional fitting technique based on the addition of bands of which the position (wavenumber), width (more precisely the full width at half maximum, FWHM) and intensity can be either assigned fixed values or free (unconstrained) in order to consistently investigate all the glass spectra. In wavenumber regions where band shift and/or broadening are observed with increasing WO_3 content (at constant TiO_2), we kept the introduced function's wavenumber and/or FWHM respectively

parameter-free. Thus, the bands A, H and M were fully unconstrained, while bands F and L were introduced with fixed FWHM values and bands D and J with fixed wavenumbers values. The remaining bands B, C, E, G, I and K were introduced with fixed wavenumber and FWHM values.

As can be seen in Fig. 6, the features shown by the set of vibrational modes of Te–O bonds in asymmetric and nearly symmetric Te–O–Te bridges (bands E-J), compared to those of pure TeO_2 glass, have only been slightly modified in terms of their bands' profiles, positions and intensity ratios upon increasing WO_3 content. The key information with respect to the crosslinking of Te–O–Te bridges within the glass network is contained within the 400-550 cm^{-1} range (bands E and F). In this region, the intensity barely decreases suggesting that the network of Te–O–Te bridges has been only slightly modified. Thus, it seems that adding WO_3 does not considerably alter the original structural features within the network of Te–O–Te bridges.

In order to exclude the compositional effect, we have calculated the normalized intensities of the decomposed bands E–H by dividing their areas by TeO_2 molar content (attributed to vibrations of Te–O bonds) and those of the bands D and K–M by WO_3 molar content (attributed to vibrations of W–O bonds). It should be noted that this approach of normalization to the composition yields dissimilar band evolutions compared to the total-area averaged spectra (*cf.* bands D, L and M for example). The compositional-dependence of the normalized intensities of bands D, E–H and K–M in TT5Wy glasses is plotted in Fig. 7.

Regarding the TeO_2-rich network, the evolution of the normalized intensities of bands E-G suggests a minor structural modification of the glass network since the bands F and G seem to be unaffected upon adding WO_3. The band E shows a moderate increase of its normalized intensity that might be due to a slightly increasing number of nearly symmetric Te–O–Te bridges. Given the relatively insignificant modification of the crosslinked network of Te–O–

Te bridges, and in agreement with the forthcoming discussion on WO_3 effect, we assign the increasing intensity of bands I and J (attributed to vibrations of Te–O and W–O bonds) to an increase of W–O–W bridges as in γ-WO_3. Since these two bands are highly interactive via overlapping, we intentionally omitted their compositional evolutions from Fig. 7.

Let us know consider the Raman bands D, K, L and M associated with distorted WO_6 octahedra. The normalized intensity decrease of the bands D, L and M upon increasing WO_3 content implies that less and less short W–O bonds (shorter than ~1.80 Å) exist in the network. In other words, less and less uniformly dispersed WO_6 octahedra are directly connected to the glass network. In fact, the normalized intensity increase of the band K suggests a possible increase of the number of corner-sharing WO_6 octahedra as in γ-WO_3 (also supported by Sekiya *et al.* [29] in TeO_2-WO_3 glasses). It is important to stress that given the small size and minor contribution of the band K, the previous discussion on its evolution is more of a hypothetical nature. Therefore, it seems that the intensity increase of the large shoulder within the 700-820 cm^{-1} range (Fig. 5) arises from vibrating W–O–W bridges in the continuously growing amorphous WO_3-like regions upon increasing WO_3 content. It is important to recall that within this wavenumber range, symmetric and asymmetric stretching vibrational modes of W–O–W bridges are expected in γ-WO_3 at ~715 and 820 cm^{-1} respectively (*cf.* Raman spectrum in Fig. 5). Moreover, the weak intensity increase in the 200-300 cm^{-1} range is probably due to bending vibrational modes of WO_6 octahedra as observed in γ-WO_3. These findings are in agreement with XPS results [55] showing a decrease of O1s binding energy in (100-x)TeO_2-xWO_3 glasses from x = 5 to 30 mol.%, which indicates that oxide ions are more likely to participate within the glass network as bridging ones.

Concerning the evolution of the boson peak (band A), the position of its maximum intensity insignificantly red-shifts accompanied with an intensity decrease with addition of TiO_2 or WO_3 contents (*cf.* Figs. 4 and 6). According to previous works [56,57], the evolution of boson

peak's position and intensity in TTxWy glasses could suggest a slight crosslinking density increase in the glass network at the medium-range scale. This behavior is in agreement with the continuous increase of the glass transition temperature upon adding TiO_2 or WO_3.

Since the same compositional evolutions of structural features as revealed by micro-Raman spectroscopy are observed upon increasing WO_3 content at different TiO_2 concentrations with no further emerging bands (Fig. 5), it seems unlikely that Ti–O–W bridges participate in the crosslinking within the glass network.

From the above discussion, we argue that unlike the peculiar structural effect of TiO_2 promoting a phase separation within the amorphous glass network, the incorporation of WO_3 results in uniformly dispersed (throughout the glass network) WO_6 octahedra which tend to form amorphous WO_3-like regions before ending with crystallized γ-WO_3 at 30 mol.%. This might explain why the addition of TiO_2 and WO_3 results in relatively moderate thermal stabilities of TTxWy glasses.

3.4 Linear optical properties

3.4.1 Refractive index, optical band gap and Urbach energies by UV-Vis-NIR optical transmission

The optical transmission spectra of 14 out of 15 TTxWy glass samples show a transparency over 75% in the 800-2600 nm range (*cf.* Fig. 8). Only the sample TT15W25 showed a markedly lower transparency of ~68% in this region. This can be related to its peculiar composition (richest in both TiO_2 and WO_3 oxides) at the boundary of the glass-forming domain. The large absorption band onsetting at ~2800 nm is recorded in all of the samples. It corresponds to the stretching mode of bound hydroxyl groups (R–OH), and both symmetric

and asymmetric stretching modes of H_2O molecules [58]. Similar evolutions are generally observed upon adding TiO_2 (or WO_3) at constant WO_3 (or TiO_2) content. Therefore, in the following, we only consider TTxW5 and TT5Wy sets when discussing the effects of TiO_2 and WO_3 on the optical properties.

The UV absorption edge red-shifts with increasing WO_3 content (*cf.* Fig. 8 (a) for TT5Wy glasses). Likewise, a minor red-shift is observed within a narrower wavelength range (400-475 nm) upon adding TiO_2. The color evolution of glass samples (described in *section 3.1*) is in agreement with the detected red-shifts of the absorption edge.

The refractive indices were extracted from the optical transmission data in the transparent region using the following equation: $T = 2n/(n^2+1)$. We provide in Table 1 the refractive indices $n_{1.5}$ at $\lambda = 1.5$ μm (typical wavelength used for optical communication). The $n_{1.5}$ indices of TT5Wy glasses are plotted in Fig. 8 (b) against WO_3 content. In general, the results suggest a practically constant behavior of the refractive index upon adding TiO_2 or WO_3 with high values ranging between ~2.10 and ~2.15. It should be stressed that the above equation slightly underestimates the refractive index value since the multiple reflections of light are neglected and most of the reflection is considered to occur at the two air/glass interfaces (Fresnel reflection). The actual refractive indices will then be provided from the ellipsometric measurements.

We have extracted the optical band gap energy E_g for all TTxWy glasses from their respective UV absorption edges. Based on the wavelength-dependence of the absorption coefficient α (*cf.* Fig. 9 (a) for TT5Wy glasses), we plotted $(\alpha h\nu)^{½}$ versus the incident photon energy hν (commonly known as Tauc plot) to estimate E_g (Fig. 9 (b) and Table 1). Decreasing E_g upon adding WO_3 in different TeO_2-based systems has been previously reported [59,60]. In agreement with literature, a slight decrease of E_g is recorded upon increasing WO_3 content from 5 mol.% (2.88 eV in TT5W5) to 25 mol.% (2.74 eV in TT5W25). Upon adding TiO_2,

E_g tends towards a marginal decrease in WO_3-poor compositions (TTxW5) and seems to remain constant in WO_3-rich ones (TTxW25).

Moreover, we have extracted the Urbach energy E_U values. E_U is characteristic of the width of the band-tails at the top of the valence band and the bottom of the conduction band, thus estimating the density of localized states [61]. A highly disordered glass network features a higher density of localized states in the band gap and thus having a high E_U value. The E_U value is obtained from the inverse of the slope of the straight line by plotting ln(α) against hν. For TTxWy glasses, the E_U values are gathered in Table 1 and lie in the range 0.096–0.108 eV. E_U is found to remain globally stable with increasing WO_3 content (~0.106 eV in TT5Wy glasses). However, a slight decrease is observed upon adding TiO_2 at constant WO_3 content (for instance from 0.105 to 0.096 eV in TTxW5 glasses). Ghribi *et al.* [62] recently reported the same behavior in (100-x-y)TeO_2-xTiO_2-yZnO glasses, namely decreasing E_U from 0.105 eV (at x = 5 and y = 15) to 0.097 eV (at x = 10 and y = 15). It is also worth mentioning that our estimated E_U values are very close to those reported in literature for WO_3-containing TeO_2-based glasses [38]. Therefore, it can be argued that adding TiO_2 to the TeO_2-rich network does not induce any significant structural modification of the glass network but instead, considering the compositional dependence of E_U, its incorporation might "lessen" the average structural disorder. In this connection, it is important to recall that upon adding TiO_2, we found the glass forming ability to be substantially reduced due to the crystallization of rutile TiO_2 in TT20Wy samples.

3.4.2 Refractive index dispersion by ellipsometry

From the dispersion curves of TTxWy glasses measured by spectroscopic ellipsometry (Fig. 10 for TT5Wy glasses), we derived the refractive indices n_∞ (*cf.* Table 1) extrapolated to

infinite wavelength using the following Sellmeier's dispersion formula [63,64]: $n = (A + B/(1-C/\lambda^2) + D/(1-E/\lambda^2))^{1/2}$ where A-E are fitting constants specific to each sample, allowing to determine $n_\infty = (A + B + D)^{1/2}$. An excellent fitting quality was achieved as demonstrated by the R^2 coefficients ranging between 0.9984 and 0.9999. The dependence of n_∞ on TiO_2 content suggests a steady evolution from an average value of ~2.187 in TT5Wy to 2.199 in TT15Wy glasses with the highest value ($n_\infty \approx 2.206$) recorded from the TT15W15 composition. Adding WO_3 results in a steady behavior with an average value of ~2.193 in TTxW5 and TTxW25. A similar steady evolution of refractive indices is observed in binary TeO_2-TiO_2 and TeO_2-WO_3 glasses [65] with n = 2.211–2.226 from 5 to 15 mol.% upon adding TiO_2 and n = 2.211–2.219 from 10 to 30 mol.% upon adding WO_3 respectively.

From optical transmission and ellipsometric measurements, the refractive index remains practically constant upon adding TiO_2 and WO_3. This behavior is coherent with the results of the structural analysis (elaborated in *section 3.3.*) that incorporating TiO_2 or WO_3 in the TeO_2-rich network does not markedly alter the inherent structural features of Te–O–Te bridges. In contrast, when the structural depolymerization takes place (*e.g.,* in presence of MgO, ZnO, BaO [66]), the refractive index progressively decreases upon adding the network modifiers.

3.4.3 Bond network nature from the dispersion energy and electronic polarizability

By applying the single-effective-oscillator model of Wemple and DiDomenico [67] to the refractive index dispersion data, we extracted optical constants that are closely connected with the bond network nature. According to this model, the refractive index dispersion can be interpreted using the following equation: $\frac{1}{n^2-1} = \frac{E_0}{E_d} - \frac{(h\nu)^2}{E_0 E_d}$. By plotting $1/(n^2-1)$ as a function of $(h\nu)^2$ and fitting a straight line, oscillator parameters E_d (dispersion energy) and E_0 (single oscillator energy) can be determined. In fact, E_d was found to obey the following empirical

relationship in more than 100 ionic and covalent crystals [67]: $E_d = \beta.N_c.Z_a.N_e$, where β parameter approaches 0.37 ± 0.05 eV and 0.26 ± 0.04 eV in covalent and ionic crystals respectively, N_c is the coordination number of the cation, Z_a the absolute charge number of the anion and N_e the total number of valence electrons per anion. Since the overall glass network structure (especially that of TeO_2-rich network) is only slightly altered upon adding TiO_2 or WO_3 (*section 3.3.*), we consider the short-range N_c parameter in TTxWy glasses to be slightly increasing upon substituting TeO_2 with TiO_2 or WO_3 since globally, Te^{4+} cations are four-fold coordinated while Ti^{4+} and W^{6+} cations are six-fold coordinated.

E_d and E_0 values lie in the range 26.11–30.37 eV and 6.93–7.99 eV respectively (Table 1). They are found to show an overall decrease with increasing TiO_2 and WO_3 contents. From the above equation, it is rational to assign this trend to a decreasing β parameter. Hence, we suggest that this evolution is associated with an ionic character amplification of the glass network, which can simply be supported by the expected ionicity increase upon substituting Te with Ti and W transition metals.

Moreover, we have calculated the electronic polarizability of oxide ions α_{O2-} based on optical band gap energies. The used method is based on the Lorentz-Lorenz equation [68,69]: $R_M = [(n^2-1)/(n^2+2)]\ V_M = (4/3)\ \pi\ N_A\ \alpha_M = 2.52\ \alpha_M$, where R_M is the molar refraction, n the refractive index, V_M the molar volume, α_M the molar polarizability and N_A the Avogadro's number. This equation allows to calculate α_{O2-} in oxide materials by subtracting the cation polarizability (considered as constant) from α_M. Following the polarizability approach developed by Dimitrov and Komatsu [70], we calculated for TTxWy glasses the α_{O2-} based on E_g using the following equation: $\alpha_{O2-} = \{(V_M/2.52)\ [1 - (E_g^{½} - 0.98)/1.23] - \sum p\alpha_i\}\ q^{-1}$, where p and q are the numbers of cations and oxide ions in the chemical formula of the oxide A_pO_q. The free-cation polarizability α_i values of Te^{4+} (1.595 $Å^3$), Ti^{4+} (0.184 $Å^3$) and W^{6+} (0.147 $Å^3$) ions were collected from ref. [70]. The obtained results are listed in Table 1.

The calculated α_{O2-} values are comprised between $\alpha_{O2-(min)}$ = 1.56 $Å^3$ and $\alpha_{O2-(max)}$ = 1.82 $Å^3$. It is found that upon adding WO_3 from 5 to 25 mol.%, α_{O2-} slightly increases from ~1.6 to ~1.8 $Å^3$ while remaining practically constant with addition of TiO_2. This slight increase of α_{O2-} values indicates that the overall glass network becomes slightly more "polarized", and thus a little more ionic in nature.

4. Conclusions.

A new TeO_2-based glass-forming domain has been explored and investigated within the ternary TeO_2-TiO_2-WO_3 system. Density, thermal, structural and linear optical properties have been measured and analyzed as a function of TiO_2 and WO_3 contents.

The structural properties of TTxWy glasses were examined using micro-Raman spectroscopy to highlight the structural roles and effects of adding TiO_2 and WO_3 on the short- to medium-range structure. We report the following structural trends:

- Globally, only minor structural modifications are taking place upon adding TiO_2 or WO_3, ***(i)*** indicating that TTxWy glasses collectively share common features of the pure TeO_2 glass network and ***(ii)*** suggesting the absence of Te–O–Te bond network depolymerization (induced transformation of TeO_4 into TeO_3 units).
- Upon adding TiO_2, we argue that a phase separation occurs between amorphous TeO_2-network and amorphous "rutile-like" TiO_2-rich regions (assumed to be of a nanometric size) in binary TTx and ternary TTxWy glasses. Therefore, it seems unlikely that hybrid Te–O–Ti bridges build the bond network in these glasses, thus explaining the limited glass-forming domain to only 15 mol.%.

- Upon adding WO_3, we argue that ***(i)*** only a minor change affects the crosslinked network of Te–O–Te bridges; ***(ii)*** at low WO_3 contents, uniformly dispersed WO_6 octahedra exist in the glass network; and ***(iii)*** at higher WO_3 contents, amorphous WO_3-like regions continuously grow before the crystallization of γ-WO_3 at 30 mol.% of WO_3. Let us recall that Sekiya *et al.* [29] have suggested the same scenario for TeO_2-WO_3 glasses.

It is important to emphasize that even though these Raman spectroscopy-based findings support the presence of distinct regions as a result of adding TiO_2 and WO_3, they still do not provide a direct proof of their actual existence. In this regard, we aim in the future to probe the existence of such regions using transmission electron microscopy.

The linear optical properties of TTxWy glasses were measured by the UV-Vis-NIR optical transmission and spectroscopic ellipsometry. In general, the obtained results suggest a steady evolution of the optical properties upon adding TiO_2 or WO_3 which is consistent with the only minor structural modifications within the TTxWy glasses. The latter possess high refractive index values ($n_{\infty(min)}$= 2.173 and $n_{\infty(max)}$= 2.206) that remain practically constant upon adding TiO_2 or WO_3. The evolution of the dispersion energy suggests a slight increase of the network's ionicity upon substituting TeO_2 with TiO_2 and WO_3, which is in agreement with the observed slight increase of the electronic oxide ion polarizability.

As a future work, this evolving bond network nature could be verified by deriving the splitting of the longitudinal optical and transverse optical (LO-TO) modes by means of infrared reflectance spectroscopy.

Acknowledgements.

We thank Dr. J. Cornette and Dr. R. Mayet for valued assistance with Raman and XRD experiments respectively. M.R. Zaki gratefully acknowledges the financial support from Conseil Régional du Limousin.

Figure captions.

Fig. 1. (a) Glass-forming domain obtained within the (100-x-y)TeO_2-xTiO_2-yWO_3 system (labeled TTxWy) surrounded by the yellow frame. Blue and green colored squares and spots correspond to partially crystallized samples in TiO_2 and WO_3 respectively. (b) Photograph of the obtained glass pellets in their final polished state. The relative positions of pellets are in accord with the black spots in the glass-forming domain.

Fig. 2. DSC curves of TT5Wy glasses. The glass transition and onset crystallization temperatures are given in bold and non-bold typefaces respectively.

Fig. 3. Total-area averaged Raman spectra of TTx glasses (x = 0, 2.5, 5, 10 and 15) along with the spectrum of $TiTe_3O_8$ (from [22]). The inset is adapted from Fig. 2 in ref. [44] and shows spectra recorded from rutile TiO_2 samples with different average crystallite sizes ranging from 5 nm up to the bulk.

Fig. 4. Evolution of total-area averaged Raman spectra of TTxWy glasses as a function of TiO_2 content. The low-wavenumber (boson peak) and mid- to high-wavenumber regions are supplied apart for more clarity.

Fig. 5. Evolution of total-area averaged Raman spectra of TTxWy glasses as a function of WO_3 content. The low-wavenumber (boson peak) and mid- to high-wavenumber regions are supplied apart for more clarity. The Raman spectrum of γ-WO_3 is reproduced from Fig. 2 in ref. **[71]**.

Fig. 6. Total-area averaged Raman spectra of TT5Wy glasses. The labels A-M correspond to the inserted bands for spectral decomposition. Inset: measured Raman spectrum of pure TeO_2 glass featuring the three major broad bands (E+F, G+H and I+J).

Fig. 7. Compositional dependence of the normalized intensities of inserted bands for the Raman spectral decomposition of TT5Wy glasses. The areas of bands E–H were divided by the TeO_2 content; those of bands D and K–M by the WO_3 content (see text).

Fig. 8. UV-Vis-NIR light transmission spectra of TTxWy glasses. Insets for TT5Wy: (a) Zoom-in plot of the UV absorption edge; (b) Compositional dependence of the refractive index calculated at 1.5 µm.

Fig. 9. (a) Evolution of the absorption coefficient as a function of the incident wavelength in TT5Wy. (b) Tauc's plot for the optical band gap energy derived from the absorption coefficient in TT5Wy.

Fig. 10. Refractive index dispersion of TT5Wy glasses. Each dispersion curve corresponds to the average of three measurements from different spots on the same glass pellet. The given refractive index values are obtained by fitting the curves using Sellmeier's equation [63]. Inset: compositional dependence of the refractive index.

Table captions.

Table 1. Thermal properties, densities and linear optical properties of TTxWy glasses. * Refractive indices obtained at λ = 1.5 μm from transmission spectra. § Refractive indices derived from ellipsometric dispersion curves using Sellmeier's equation.

Table 2. Wavenumbers and vibrational assignments of the inserted bands. Raman bands arising from TeO_2 network (Te–O–Te bridges) and their assignments are highlighted in bold typeface. In the spectral decomposition process, the wavenumbers of F, H, L and M bands were unconstrained and are given herein as wavenumber ranges in TT5Wy glasses.

References.

[1] S.-H. Kim, T. Yoko, S. Sakka, Linear and nonlinear optical properties of TeO_2 glass, J. Am. Ceram. Soc. 76 (1993) 2486–2490. doi:10.1111/j.1151-2916.1993.tb03970.x.

[2] V. Dimitrov, S. Sakka, Linear and nonlinear optical properties of simple oxides. II, J. Appl. Phys. 79 (1996) 1741–1745. doi:10.1063/1.360963.

[3] R.A.H. El-Mallawany, Tellurite glasses handbook: physical properties and data, 2nd ed, Taylor & Francis, Boca Raton, FL, 2011.

[4] J.C. Champarnaud-Mesjard, S. Blanchandin, P. Thomas, A. Mirgorodsky, T. Merle-Méjean, B. Frit, Crystal structure, Raman spectrum and lattice dynamics of a new metastable form of tellurium dioxide: γ-TeO_2, J. Phys. Chem. Solids. 61 (2000) 1499–1507. doi:10.1016/S0022-3697(00)00012-3.

[5] O. Noguera, T. Merle-Méjean, A.P. Mirgorodsky, M.B. Smirnov, P. Thomas, J.-C. Champarnaud-Mesjard, Vibrational and structural properties of glass and crystalline phases of TeO_2, J. Non-Cryst. Solids. 330 (2003) 50–60. doi:10.1016/j.jnoncrysol.2003.08.052.

[6] E. Fargin, A. Berthereau, T. Cardinal, G. Le Flem, L. Ducasse, L. Canioni, P. Segonds, L. Sarger, A. Ducasse, Optical non-linearity in oxide glasses, J. Non-Cryst. Solids. 203 (1996) 96–101. doi:10.1016/0022-3093(96)00338-9.

[7] B. Jeansannetas, S. Blanchandin, P. Thomas, P. Marchet, J.C. Champarnaud-Mesjard, T. Merle-Méjean, B. Frit, V. Nazabal, E. Fargin, G. Le Flem, M.O. Martin, B. Bousquet, L. Canioni, S. Le Boiteux, P. Segonds, L. Sarger, Glass structure and optical nonlinearities in thallium(I) tellurium(IV) oxide glasses, J. Solid State Chem. 146 (1999) 329–335. doi:10.1006/jssc.1999.8355.

[8] S. Suehara, P. Thomas, A. Mirgorodsky, T. Merle-Méjean, J.C. Champarnaud-Mesjard, T. Aizawa, S. Hishita, S. Todoroki, T. Konishi, S. Inoue, Non-linear optical properties of TeO_2-based glasses: ab initio static finite-field and time-dependent calculations, J. Non-Cryst. Solids. 345–346 (2004) 730–733. doi:10.1016/j.jnoncrysol.2004.08.191.

[9] S. Suehara, P. Thomas, A.P. Mirgorodsky, T. Merle-Méjean, J.C. Champarnaud-Mesjard, T. Aizawa, S. Hishita, S. Todoroki, T. Konishi, S. Inoue, Localized hyperpolarizability approach to the origin of nonlinear optical properties in TeO_2-based materials, Phys. Rev. B. 70 (2004). doi:10.1103/PhysRevB.70.205121.

[10] E.M. Roginskii, V.G. Kuznetsov, M.B. Smirnov, O. Noguera, J.-R. Duclère, M. Colas, O. Masson, P. Thomas, Comparative Analysis of the Electronic Structure and Nonlinear Optical Susceptibility of α-TeO_2 and β-TeO_3 Crystals, J. Phys. Chem. C. 121 (2017) 12365−12374. doi:10.1021/acs.jpcc.7b01819.

[11] A.P. Mirgorodsky, M. Soulis, P. Thomas, T. Merle-Méjean, M. Smirnov, Ab initio study of the nonlinear optical susceptibility of TeO_2-based glasses, Phys. Rev. B. 73 (2006) 134206. doi:10.1103/PhysRevB.73.134206.

[12] M. Soulis, T. Merle-Méjean, A.P. Mirgorodsky, O. Masson, E. Orhan, P. Thomas, M.B. Smirnov, Local molecular orbitals and hyper-susceptibility of TeO_2 glass, J. Non-Cryst. Solids. 354 (2008) 199–202. doi:10.1016/j.jnoncrysol.2007.07.036.

[13] M. Smirnov, A. Mirgorodsky, O. Masson, P. Thomas, Quantum mechanical study of pre-dissociation enhancement of linear and nonlinear polarizabilities of $(TeO_2)_n$ oligomers as a key to understanding the remarkable dielectric properties of TeO_2 glasses, J. Phys. Chem. A. 116 (2012) 9361–9369. doi:10.1021/jp303014k.
[14] M.E. Lines, Influence of d orbitals on the nonlinear optical response of transparent transition-metal oxides, Phys. Rev. B. 43 (1991) 11978–11990. doi:10.1103/PhysRevB.43.11978.
[15] S.-H. Kim, T. Yoko, Nonlinear optical properties of TeO_2-based glasses: MO_x-TeO_2 (M= Sc, Ti, V, Nb, Mo, Ta, and W) binary glasses, J. Am. Ceram. Soc. 78 (1995) 1061–1065. doi:10.1111/j.1151-2916.1995.tb08437.x.
[16] T. Sekiya, N. Mochida, A. Ohtsuka, M. Tonokawa, Raman spectra of $MO_{1/2}$-TeO_2 (M= Li, Na, K, Rb, Cs and Tl) glasses, J. Non-Cryst. Solids. 144 (1992) 128–144. doi:10.1016/S0022-3093(05)80393-X.
[17] J.C. McLaughlin, S.L. Tagg, J.W. Zwanziger, The structure of alkali tellurite glasses, J. Phys. Chem. B. 105 (2001) 67–75. doi:10.1021/jp0025779.
[18] N. Berkaïne, J. Cornette, D. Hamani, P. Thomas, O. Masson, A. Mirgorodsky, M. Colas, J. Duclère, T. Merle-Mejéan, J.-C. Champarnaud-Mesjard, M. Smirnov, Structure and dielectric properties of tellurium oxide-based materials, Adv. Electroceramic Mater. II. (2010) 63–74. doi:10.1002/9780470930915.ch7.
[19] G. Upender, C.P. Vardhani, S. Suresh, A.M. Awasthi, V. Chandra Mouli, Structure, physical and thermal properties of WO_3–GeO_2–TeO_2 glasses, Mater. Chem. Phys. 121 (2010) 335–341. doi:10.1016/j.matchemphys.2010.01.050.
[20] H. Fares, I. Jlassi, H. Elhouichet, M. Férid, Investigations of thermal, structural and optical properties of tellurite glass with WO_3 adding, J. Non-Cryst. Solids. 396–397 (2014) 1–7. doi:10.1016/j.jnoncrysol.2014.04.012.
[21] J.C. Sabadel, P. Armand, D. Cachau-Herreillat, P. Baldeck, O. Doclot, A. Ibanez, E. Philippot, Structural and nonlinear optical characterizations of tellurium oxide-based glasses: TeO_2–BaO–TiO_2, J. Solid State Chem. 132 (1997) 411–419. doi:10.1006/jssc.1997.7499.
[22] M. Soulis, A.P. Mirgorodsky, T. Merle-Méjean, O. Masson, P. Thomas, M. Udovic, The role of modifier's cation valence in structural properties of TeO_2-based glasses, J. Non-Cryst. Solids. 354 (2008) 143–149. doi:10.1016/j.jnoncrysol.2007.07.032.
[23] M. Udovic, P. Thomas, A. Mirgorodsky, O. Masson, T. Merle-Mejean, C. Lasbrugnas, J.C. Champarnaud-Mesjard, T. Hayakawa, Formation domain and characterization of new glasses within the Tl_2O–TiO_2–TeO_2 system, Mater. Res. Bull. 44 (2009) 248–253. doi:10.1016/j.materresbull.2008.10.001.
[24] M. Udovic, P. Thomas, A. Mirgorodsky, O. Durand, M. Soulis, O. Masson, T. Merle-Méjean, J.C. Champarnaud-Mesjard, Thermal characteristics, Raman spectra and structural properties of new tellurite glasses within the Bi_2O_3–TiO_2–TeO_2 system, J. Solid State Chem. 179 (2006) 3252–3259. doi:10.1016/j.jssc.2006.06.016.
[25] N. Ghribi, M. Dutreilh-Colas, J.-R. Duclère, T. Hayakawa, J. Carreaud, R. Karray, A. Kabadou, P. Thomas, Thermal, optical and structural properties of glasses within the TeO_2-TiO_2-ZnO system, J. Alloys Compd. 622 (2015) 333–340. doi:10.1016/j.jallcom.2014.10.063.
[26] G. Meunier, J. Galy, Sur une déformation inédite du reseau de type fluorine. Structure cristalline des phases MTe_3O_8 (M = Ti, Sn, Hf, Zr), Acta Crystallogr. B. 27 (1971) 602–608. doi:10.1107/S0567740871002620.
[27] S. Blanchandin, P. Marchet, P. Thomas, J.C. Champarnaud-Mesjard, B. Frit, A. Chagraoui, New investigations within the TeO_2-WO_3 system: phase equilibrium diagram and glass crystallization, J. Mater. Sci. 34 (1999) 4285–4292. doi:10.1023/A:1004667223028.
[28] V. Dimitrov, M. Arnaudov, Y. Dimitriev, IR-spectral study of the effect of WO_3 on the structure of tellurite glasses, Monatshefte Für Chem. Chem. Mon. 115 (1984) 987–991. doi:10.1007/BF00798766.
[29] T. Sekiya, N. Mochida, S. Ogawa, Structural study of WO_3-TeO_2 glasses, J. Non-Cryst. Solids. 176 (1994) 105–115. doi:10.1016/0022-3093(94)90067-1.
[30] I. Shaltout, Y. Tang, R. Braunstein, A.M. Abu-Elazm, Structural studies of tungstate-tellurite glasses by Raman spectroscopy and differential scanning calorimetry, J. Phys. Chem. Solids. 56 (1995) 141–150. doi:10.1016/0022-3697(94)00150-2.
[31] B.V.R. Chowdari, P.P. Kumari, Studies on Ag_2O-M_xO_y-TeO_2 (M_xO_y= WO_3, MoO_3, P_2O_5 and B_2O_3) ionic conducting glasses, in: Solid State Ion., Elsevier, 1998: pp. 665–675. doi:10.1016/S0167-2738(98)00393-2.
[32] V.O. Sokolov, V.G. Plotnichenko, E.M. Dianov, Structure of WO_3-TeO_2 glasses, Inorg. Mater. 43 (2007) 194–213. doi:10.1134/S0020168507020173.
[33] G. Upender, S. Bharadwaj, A.M. Awasthi, V. Chandra Mouli, Glass transition temperature-structural studies of tungstate tellurite glasses, Mater. Chem. Phys. 118 (2009) 298–302. doi:10.1016/j.matchemphys.2009.07.058.

[34] A. Mirgorodsky, M. Colas, M. Smirnov, T. Merle-Méjean, R. El-Mallawany, P. Thomas, Structural peculiarities and Raman spectra of TeO_2-WO_3-based glasses: A fresh look at the problem, J. Solid State Chem. 190 (2012) 45–51. doi:10.1016/j.jssc.2012.02.011.
[35] A. Kaur, A. Khanna, V.G. Sathe, F. Gonzalez, B. Ortiz, Optical, thermal, and structural properties of Nb_2O_5–TeO_2 and WO_3–TeO_2 glasses, Phase Transit. 86 (2013) 598–619. doi:10.1080/01411594.2012.727998.
[36] B.O. Loopstra, P. Boldrini, Neutron diffraction investigation of WO_3, Acta Crystallogr. 21 (1966) 158–162. doi:10.1107/S0365110X66002469.
[37] V.V. Safonov, Interactions in the TeO_2-TiO_2-WO_3 system, Russ. J. Inorg. Chem. 53 (2008) 460–461. doi:10.1134/S0036023608030224.
[38] D.M. Munoz-Martín, TeO_2-based film glasses for photonic applications: structural and optical properties., PhD, Universidad Complutense de Madrid, 2010.
[39] D. De Sousa Meneses, Software utility for the creation of optical function (FOCUS), CEMHTI UPR 3079 CNRS Orléans, France, 2004. http://www.cemhti.cnrs-orleans.fr/pot/software/focus.html.
[40] S. Tanisaki, Crystal structure of monoclinic tungsten trioxide at room temperature, J. Phys. Soc. Jpn. 15 (1960) 573–581. doi:10.1143/JPSJ.15.573.
[41] A. H. Dietzel, Die kationenfeldstärken und ihre beziehungen zu entglasungsvorgängen, zur verbindungsbildung und zu den schmelzpunkten von silikaten, Z Electrochem. 48 (1942) 9–23.
[42] A.K. Varshneya, Chapter 3 - Glass formation principles, in: Fundam. Inorg. Glas., Academic Press, San Diego, 1994: pp. 27–59.
[43] R.D. Shannon, Revised effective ionic radii and systematic studies of interatomic distances in halides and chalcogenides, Acta Crystallogr. Sect. A. 32 (1976) 751–767. doi:10.1107/S0567739476001551.
[44] V. Swamy, B.C. Muddle, Q. Dai, Size-dependent modifications of the Raman spectrum of rutile TiO_2, Appl. Phys. Lett. 89 (2006) 163118. doi:10.1063/1.2364123.
[45] S. Zhou, E. Čižmár, K. Potzger, M. Krause, G. Talut, M. Helm, J. Fassbender, S.A. Zvyagin, J. Wosnitza, H. Schmidt, Origin of magnetic moments in defective TiO_2 single crystals, Phys. Rev. B. 79 (2009). doi:10.1103/PhysRevB.79.113201.
[46] I. Lukačević, S.K. Gupta, P.K. Jha, D. Kirin, Lattice dynamics and Raman spectrum of rutile TiO_2: The role of soft phonon modes in pressure induced phase transition, Mater. Chem. Phys. 137 (2012) 282–289. doi:10.1016/j.matchemphys.2012.09.022.
[47] O. Noguera, T. Merle-Méjean, A.P. Mirgorodsky, P. Thomas, J.-C. Champarnaud-Mesjard, Dynamics and crystal chemistry of tellurites. II. Composition- and temperature-dependence of the Raman spectra of $x(Tl_2O)+(1-x)\ TeO_2$ glasses: evidence for a phase separation?, J. Phys. Chem. Solids. 65 (2004) 981–993. doi:10.1016/j.jpcs.2003.11.020.
[48] S.S. Sukhov, V.N. Sigaev, P. Perniche, A. Aronne, E. Fanelli, S. Brovelli, A. Paleari, G.E. Malashkevich, Structure and properties of erbium-titanium-tellurite glass, Glass Ceram. 63 (2006) 399–402. doi:10.1007/s10717-006-0133-6.
[49] N. Gupta, A. Khanna, F. Gonzàlez, R. Iordanova, Thermal characteristics, Raman spectra, optical and structural properties of TiO_2-Bi_2O_3-B_2O_3-TeO_2 glasses, in: 2017: p. 070005. doi:10.1063/1.4980440.
[50] O. Noguera, Propriétés structurales, vibrationnelles et diélectriques de matériaux à base d'oxyde de tellure, PhD thesis, Université de Limoges, 2003.
[51] A.P. Mirgorodsky, T. Merle-Méjean, J.-C. Champarnaud, P. Thomas, B. Frit, Dynamics and structure of TeO_2 polymorphs: model treatment of paratellurite and tellurite; Raman scattering evidence for new γ- and δ-phases, J. Phys. Chem. Solids. 61 (2000) 501–509. doi:10.1016/S0022-3697(99)00263-2.
[52] T. Vasileiadis, S.N. Yannopoulos, Photo-induced oxidation and amorphization of trigonal tellurium: A means to engineer hybrid nanostructures and explore glass structure under spatial confinement, J. Appl. Phys. 116 (2014) 103510. doi:10.1063/1.4894868.
[53] Y.V. Denisov, A.A. Zubovich, Boson Peak and Medium-Range Order Structure of Alkali Borate Glasses, Glass Phys. Chem. 29 (2003) 345–352. doi:10.1023/A:1025112607893.
[54] E. Stavrou, C. Tsiantos, R.D. Tsopouridou, S. Kripotou, A.G. Kontos, C. Raptis, B. Capoen, M. Bouazaoui, S. Turrell, S. Khatir, Raman scattering boson peak and differential scanning calorimetry studies of the glass transition in tellurium–zinc oxide glasses, J. Phys. Condens. Matter. 22 (2010) 195103. doi:10.1088/0953-8984/22/19/195103.
[55] P. Charton, L. Gengembre, P. Armand, TeO_2-WO_3 glasses: Infrared, XPS and XANES structural characterizations, J. Solid State Chem. 168 (2002) 175–183. doi:10.1006/jssc.2002.9707.
[56] A.P. Sokolov, A. Kisliuk, M. Soltwisch, D. Quitmann, Medium-range order in glasses: Comparison of Raman and diffraction measurements, Phys. Rev. Lett. 69 (1992) 1540–1543. doi:10.1103/PhysRevLett.69.1540.

[57] A.G. Kalampounias, G.N. Papatheodorou, S.N. Yannopoulos, A temperature dependence Raman study of the 0.1 Nb_2O_5-0.9 TeO_2 glass-forming system, J. Phys. Chem. Solids. 67 (2006) 725–731. doi:10.1016/j.jpcs.2005.11.001.
[58] A.M. Efimov, V.G. Pogareva, A.V. Shashkin, Water-related bands in the IR absorption spectra of silicate glasses, J. Non-Cryst. Solids. 332 (2003) 93–114. doi:10.1016/j.jnoncrysol.2003.09.020.
[59] E.S. Yousef, A. El-Adawy, N. El Koshkhany, E.R. Shaaban, Optical and acoustic properties of TeO_2-WO_3 glasses with small amount of additive ZrO_2, J. Phys. Chem. Solids. 67 (2006) 1649–1655. doi:10.1016/j.jpcs.2006.02.014.
[60] M.M. Umair, A.K. Yahya, M.K. Halimah, H.A.A. Sidek, Effects of increasing tungsten on structural, elastic and optical properties of xWO_3–$(40-x)Ag_2O$–$60TeO_2$ Glass System, J. Mater. Sci. Technol. 31 (2015) 83–90. doi:10.1016/j.jmst.2014.10.002.
[61] F. Urbach, The long-wavelength edge of photographic sensitivity and of the electronic absorption of solids, Phys. Rev. 92 (1953) 1324–1324. doi:10.1103/PhysRev.92.1324.
[62] N. Ghribi, Synthèse, caractérisations structurale et élastique de nouveaux matériaux tellurites pour des applications en optique non linéaire, PhD thesis, Université de Limoges, 2015.
[63] Sellmeier, Zur Erklärung der abnormen Farbenfolge im Spectrum einiger Substanzen, Ann. Phys. Chem. 219 (1871) 272–282. doi:10.1002/andp.18712190612.
[64] G. Ghosh, Sellmeier coefficients and dispersion of thermo-optic coefficients for some optical glasses, Appl. Opt. 36 (1997) 1540. doi:10.1364/AO.36.001540.
[65] G. Dai, F. Tassone, A. LiBassi, V. Russo, C.E. Bottani, F. D'Amore, TeO_2-based glasses containing Nb_2O_5, TiO_2, and WO_3 for discrete Raman fiber amplification, IEEE Photonics Technol. Lett. 16 (2004) 1011–1013. doi:10.1109/LPT.2004.824963.
[66] S. Manning, H. Ebendorff-Heidepriem, T.M. Monro, Ternary tellurite glasses for the fabrication of nonlinear optical fibres, Opt. Mater. Express. 2 (2012) 140–152. doi:10.1364/OME.2.000140.
[67] S.H. Wemple, Refractive-index behavior of amorphous semiconductors and glasses, Phys. Rev. B. 7 (1973) 3767–3777. doi:10.1103/PhysRevB.7.3767.
[68] H.A. Lorentz, Ueber die Beziehung zwischen der Fortpflanzungsgeschwindigkeit des Lichtes und der Körperdichte, Ann. Phys. Chem. 245 (1880) 641–665. doi:10.1002/andp.18802450406.
[69] L. Lorenz, Über die Refractionsconstante, Wiedem. Ann. 11 (1880) 70.
[70] V. Dimitrov, T. Komatsu, An interpretation of optical properties of oxides and oxide glasses in terms of the electronic ion polarizability and average single bond strength, Journal of the University of Chemical Technology and Metallurgy. 45 (2010) 219–250.
[71] M.F. Daniel, B. Desbat, J.C. Lassegues, B. Gerand, M. Figlarz, Infrared and Raman study of WO_3 tungsten trioxides and WO_3, xH_2O tungsten trioxide hydrates, J. Solid State Chem. 67 (1987) 235–247. doi:10.1016/0022-4596(87)90359-8.

Table 1

Sample	T_g (°C) ±1	ΔT (°C) ±1	Density (g/cm^3)	E_g (eV) ±0.020	E_U (eV) ±0.002	$n_{1.5}$* ±0.010	n_∞ §	E_0 (eV)	E_d (eV)	α_{O2-} (Å^3)
TT5W5	328	31	5.586 ±0.003	2.880	0.105	2.132	2.195 ±0.015	7.992 ±0.126	30.371 ±1.116	1.593 ±0.048
TT5W10	341	36	5.677 ±0.008	2.842	0.105	2.127	2.188 ±0.011	7.556 ±0.169	28.523 ±1.355	1.653 ±0.053
TT5W15	355	38	5.777 ±0.007	2.789	0.106	2.122	2.186 ±0.027	7.667 ±0.233	28.792 ±3.164	1.727 ±0.047
TT5W20	365	38	5.764 ±0.006	2.764	0.105	2.141	2.173 ±0.019	7.360 ±0.156	27.230 ±2.289	1.807 ±0.052
TT5W25	376	41	5.925 ±0.008	2.744	0.107	2.118	2.191 ±0.020	7.599 ±0.174	28.669 ±2.066	1.810 ±0.055
TT10W5	353	45	5.529 ±0.009	2.843	0.100	2.112	2.185 ±0.030	7.354 ±0.190	27.583 ±2.798	1.564 ±0.047
TT10W10	364	45	5.643 ±0.010	2.812	0.103	2.123	2.197 ±0.014	7.763 ±0.132	29.545 ±1.137	1.682 ±0.060
TT10W15	376	52	5.748 ±0.008	2.776	0.103	2.128	2.182 ±0.024	7.317 ±0.189	27.333 ±2.545	1.731 ±0.055
TT10W20	389	54	5.799 ±0.006	2.758	0.103	2.133	2.191 ±0.013	7.022 ±0.095	26.519 ±0.851	1.777 ±0.066
TT10W25	399	57	5.860 ±0.004	2.736	0.108	2.134	2.190 ±0.018	6.927 ±0.090	26.106 ±1.138	1.823 ±0.046
TT15W5	380	38	5.454 ±0.004	2.826	0.096	2.120	2.198 ±0.024	7.067 ±0.119	26.851 ±1.673	1.669 ±0.045
TT15W10	391	39	5.535 ±0.004	2.800	0.102	2.140	2.198 ±0.012	7.025 ±0.115	26.659 ±1.169	1.717 ±0.040
TT15W15	405	40	5.623 ±0.008	2.782	0.100	2.113	2.206 ±0.015	7.048 ±0.081	27.027 ±0.834	1.750 ±0.046
TT15W20	414	52	5.682 ±0.007	2.761	0.103	2.116	2.196 ±0.023	7.143 ±0.162	27.132 ±2.321	1.797 ±0.035
TT15W25	426	48	5.757 ±0.005	2.758	0.100	—	2.199 ±0.011	6.987 ±0.080	26.604 ±0.809	1.813 ±0.032

Table 2

Band	Wavenumber (cm^{-1})	Raman bands assignments
A	44.0 – 45.6	• The boson peak, ascribed to an excess density of vibrational states [56].
B	146.9 *(fixed)*	• Intra-chain vibrations of Te–Te bonds (as in amorphous metallic trigonal Te) [52].
C	230 *(fixed)*	• Bending vibrations of WO_6 octahedra (as in γ-WO_3) [71].
D	351 *(fixed)*	• Bending vibrations of distorted WO_6 octahedra [71].
E	**425 *(fixed)***	• **Symmetric stretching vibrations in nearly symmetric Te–O–Te bridges (as in γ-TeO_2)** [4,51]. • Motions of oxide ions in O–Ti–O bridges along the *c* axis (E_g mode of rutile TiO_2) [46].
F	**501.8 – 505.8**	• **Symmetric stretching vibrations in Te–O–Te bridges** [4,51].
G	**607 *(fixed)***	• **Asymmetric stretching vibrations in nearly symmetric Te–O–Te bridges (as in γ-TeO_2)** [4,51]. • Motions of oxide ions in O–Ti–O bridges perpendicular to the *c* axis (A_{1g} mode of rutile TiO_2) [46].
H	**657.9 – 660.4**	• **Asymmetric stretching vibrations in asymmetric Te–O–Te bridges** [4,51].
I	**715 *(fixed)***	• **Asymmetric stretching vibrations in asymmetric Te–O–Te bridges** [4,51]. • Symmetric stretching vibrations in W–O–W bridges (as in γ-WO_3) [71].
J	**772 *(fixed)***	• **Asymmetric stretching of essentially covalent Te–$_{eq}$O bonds** [4,51].
K	820 *(fixed)*	• Asymmetric stretching vibrations in W–O–W bridges (as in γ-WO_3) [71].
L	852.3 – 863.1	• Stretching vibrations of W–O bonds in W–O–W bridges [29]. • Antisymmetric stretching vibrations of Ti–O bonds (B_{2g} mode of rutile TiO_2) [44,45].
M	925 – 934	• Asymmetric stretching vibrations of W–O bonds [71].

Figure 1

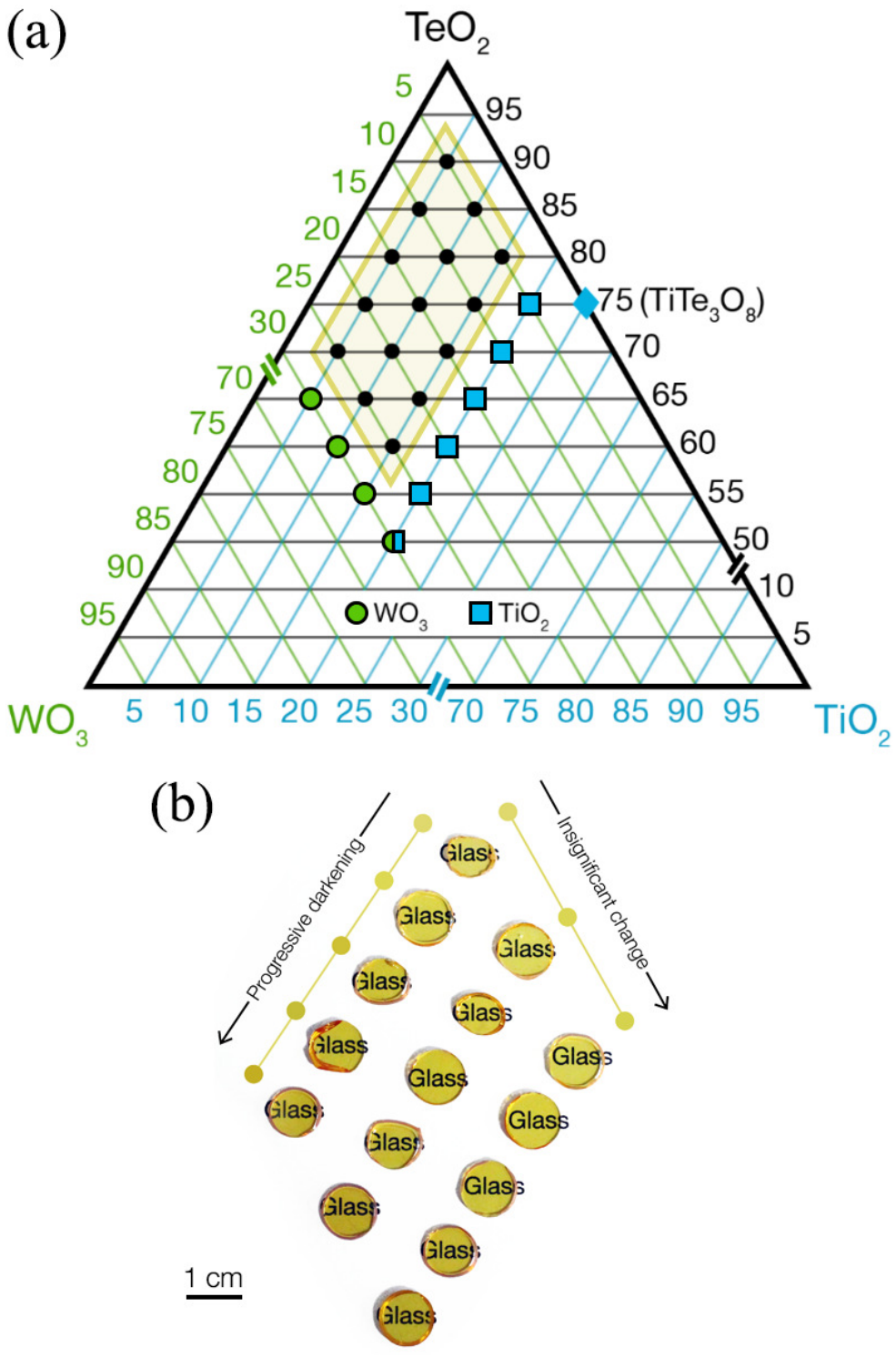
(a)
TeO2
5
10
15
20
25
30
70
75
80
85
90
95
95
90
85
80
75 (TiTe3O8)
70
65
60
55
50
10
5
WO3
TiO2
WO3 5 10 15 20 25 30 70 75 80 85 90 95 TiO2
(b)
Progressive darkening
Insignificant change
Glass
1 cm

Figure 2

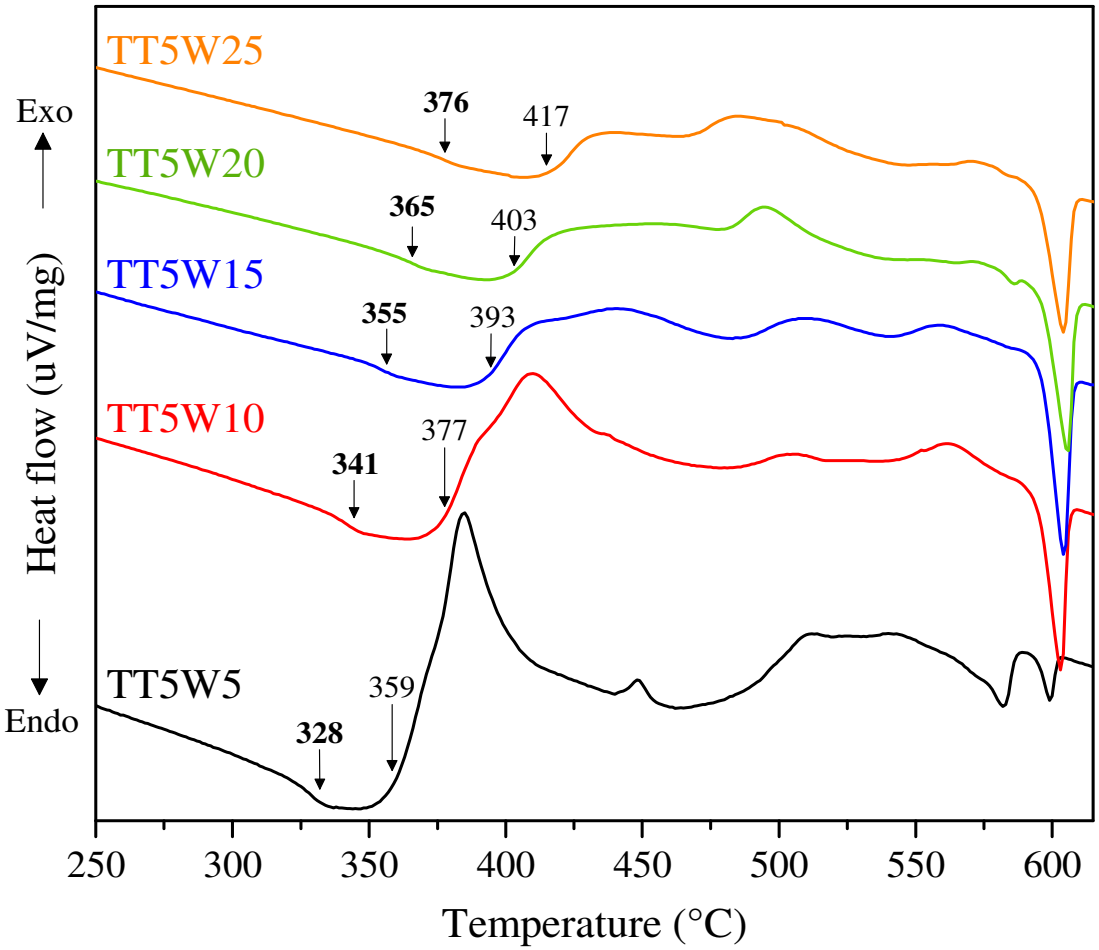
TT5W25
376
417
TT5W20
365
403
TT5W15
355
393
TT5W10
341
377
TT5W5
328
359
Exo
Endo
Heat flow (uV/mg)
250
300
350
400
450
500
550
600
Temperature (°C)

Figure 3

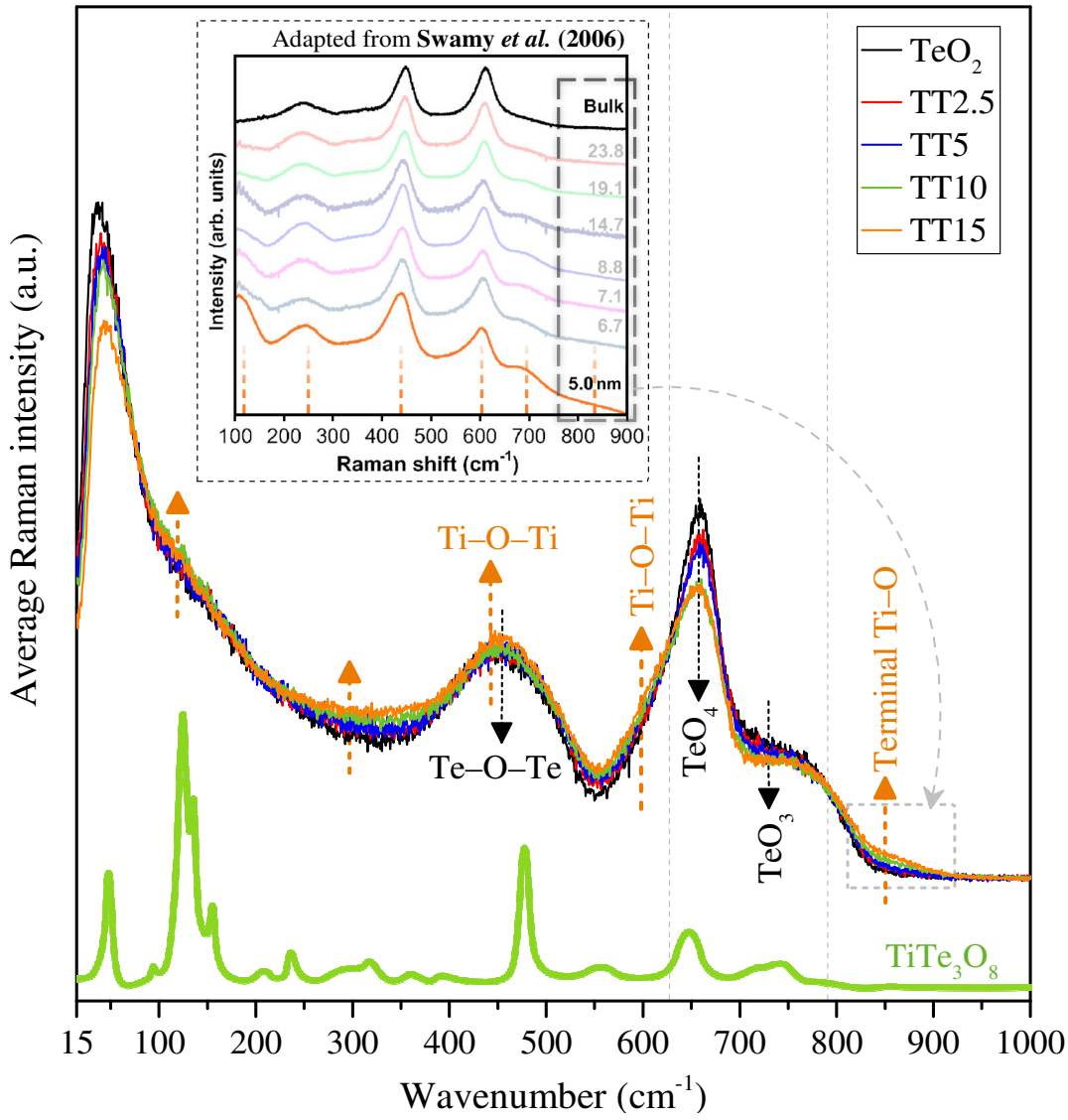
Adapted from Swamy et al. (2006)
Bulk
23.8
19.1
14.7
8.8
7.1
6.7
5.0 nm
Intensity (arb. units)
100 200 300 400 500 600 700 800 900
Raman shift (cm-1)
TeO2
TT2.5
TT5
TT10
TT15
Average Raman intensity (a.u.)
Ti–O–Ti
Te–O–Te
Ti–O–Ti
TeO4
TeO3
Terminal Ti–O
TiTe3O8
15 100 200 300 400 500 600 700 800 900 1000
Wavenumber (cm-1)

Figure 4

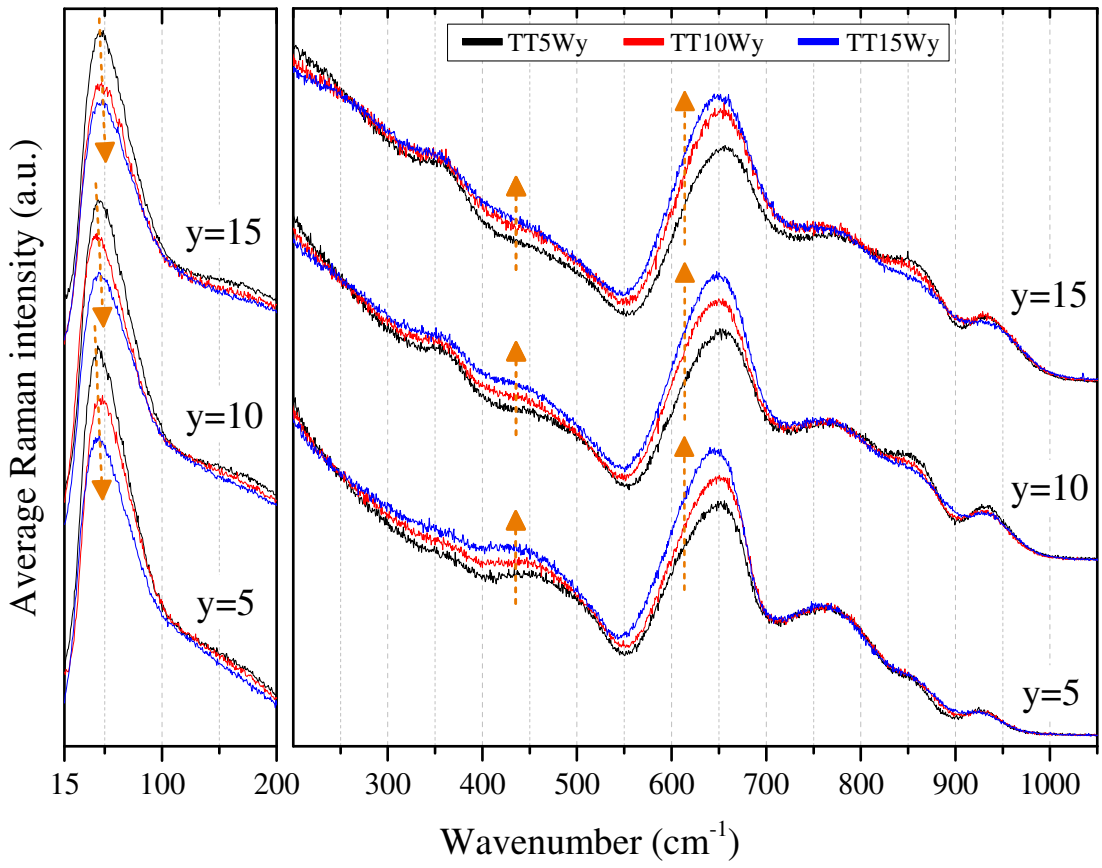
TT5Wy
TT10Wy
TT15Wy
Average Raman intensity (a.u.)
y=15
y=10
y=5
15
100
200
300
400
500
600
700
800
900
1000
Wavenumber (cm-1)

Figure 5

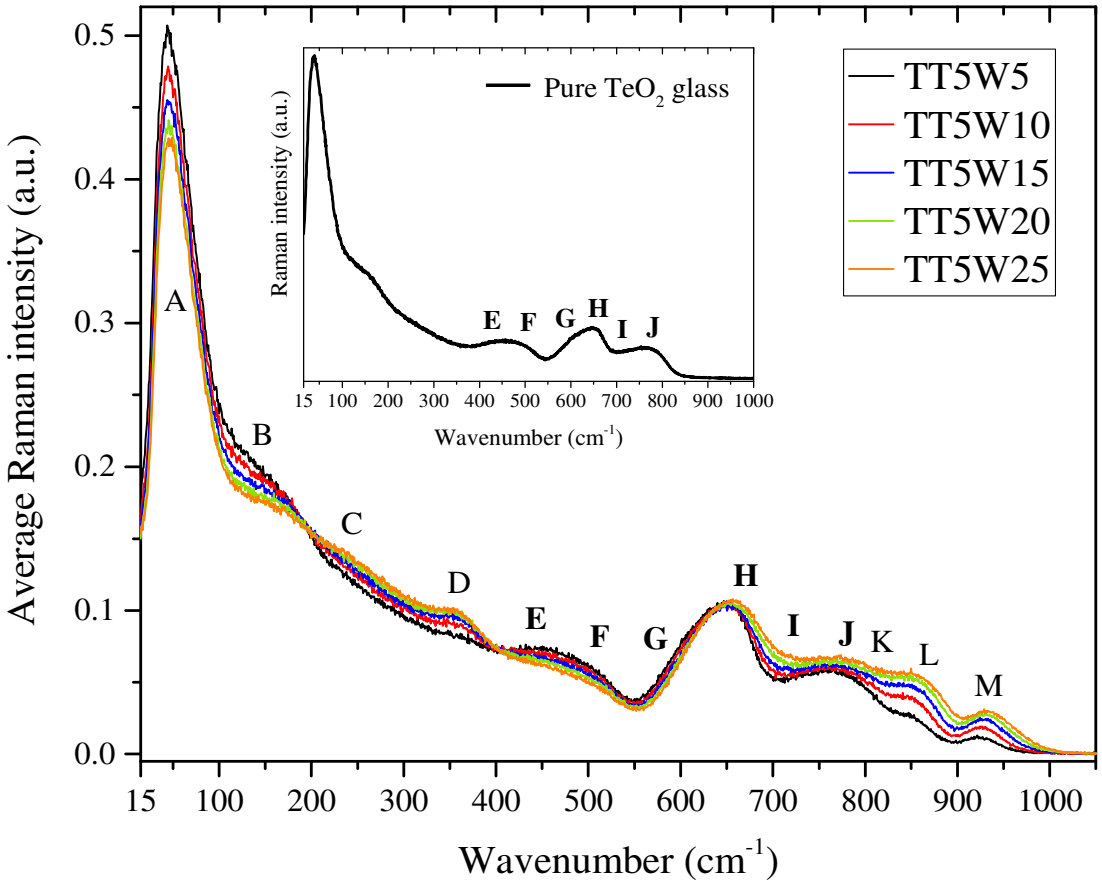
Average Raman intensity (a.u.)
Wavenumber (cm-1)
TT5W5
TT5W10
TT5W15
TT5W20
TT5W25
A
B
C
D
E
F
G
H
I
J
K
L
M
Pure TeO2 glass
Raman intensity (a.u.)
Wavenumber (cm-1)

Figure 6

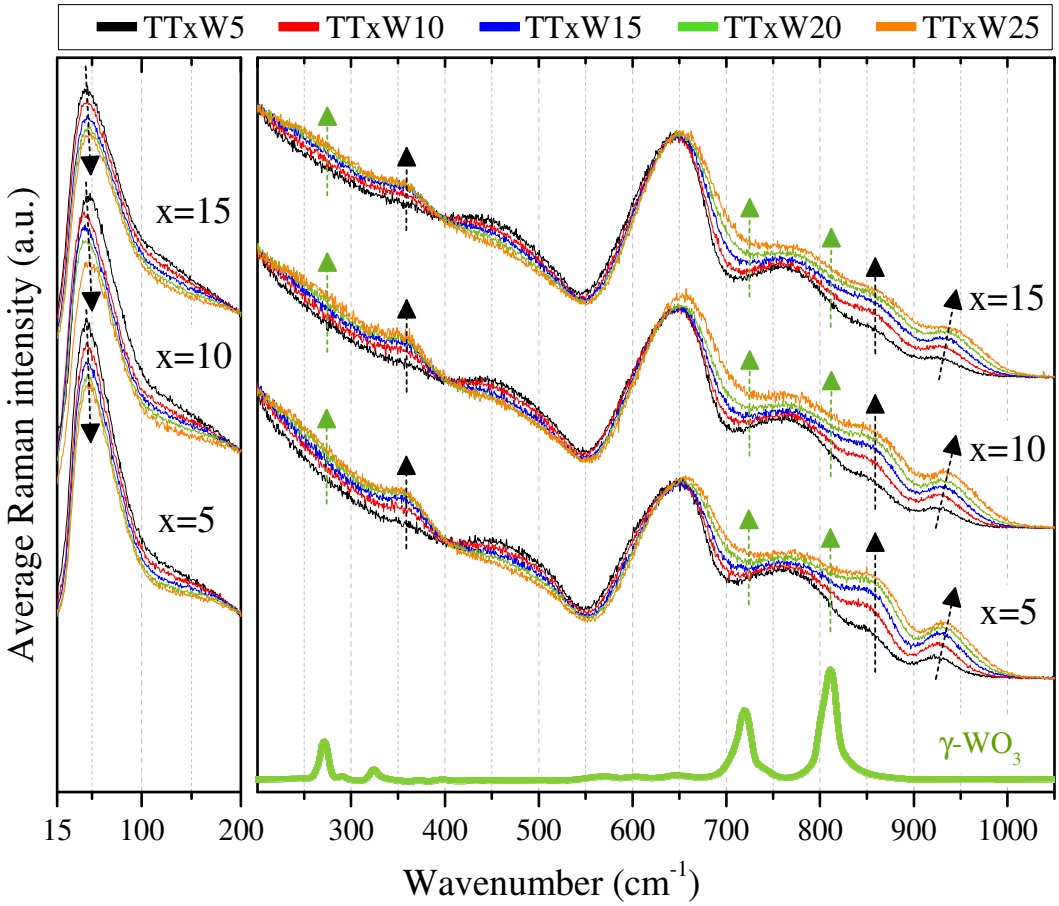
TTxW5
TTxW10
TTxW15
TTxW20
TTxW25
x=15
x=10
x=5
x=15
x=10
x=5
γ-WO3
Average Raman intensity (a.u.)
15
100
200
300
400
500
600
700
800
900
1000
Wavenumber (cm-1)

Figure 7

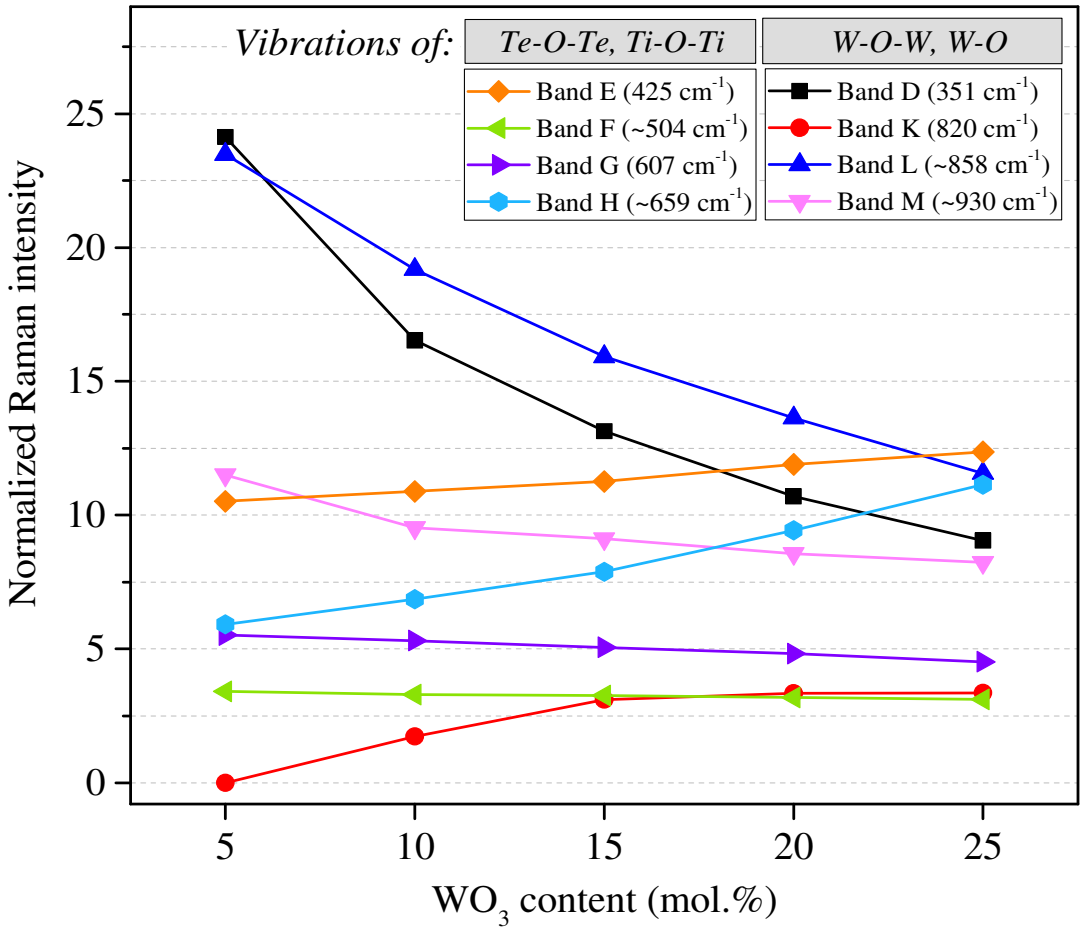
Vibrations of:
Te-O-Te, Ti-O-Ti
W-O-W, W-O
Band E (425 cm-1)
Band F (~504 cm-1)
Band G (607 cm-1)
Band H (~659 cm-1)
Band D (351 cm-1)
Band K (820 cm-1)
Band L (~858 cm-1)
Band M (~930 cm-1)
Normalized Raman intensity
0
5
10
15
20
25
5
10
15
20
25
WO3 content (mol.%)

Figure 8

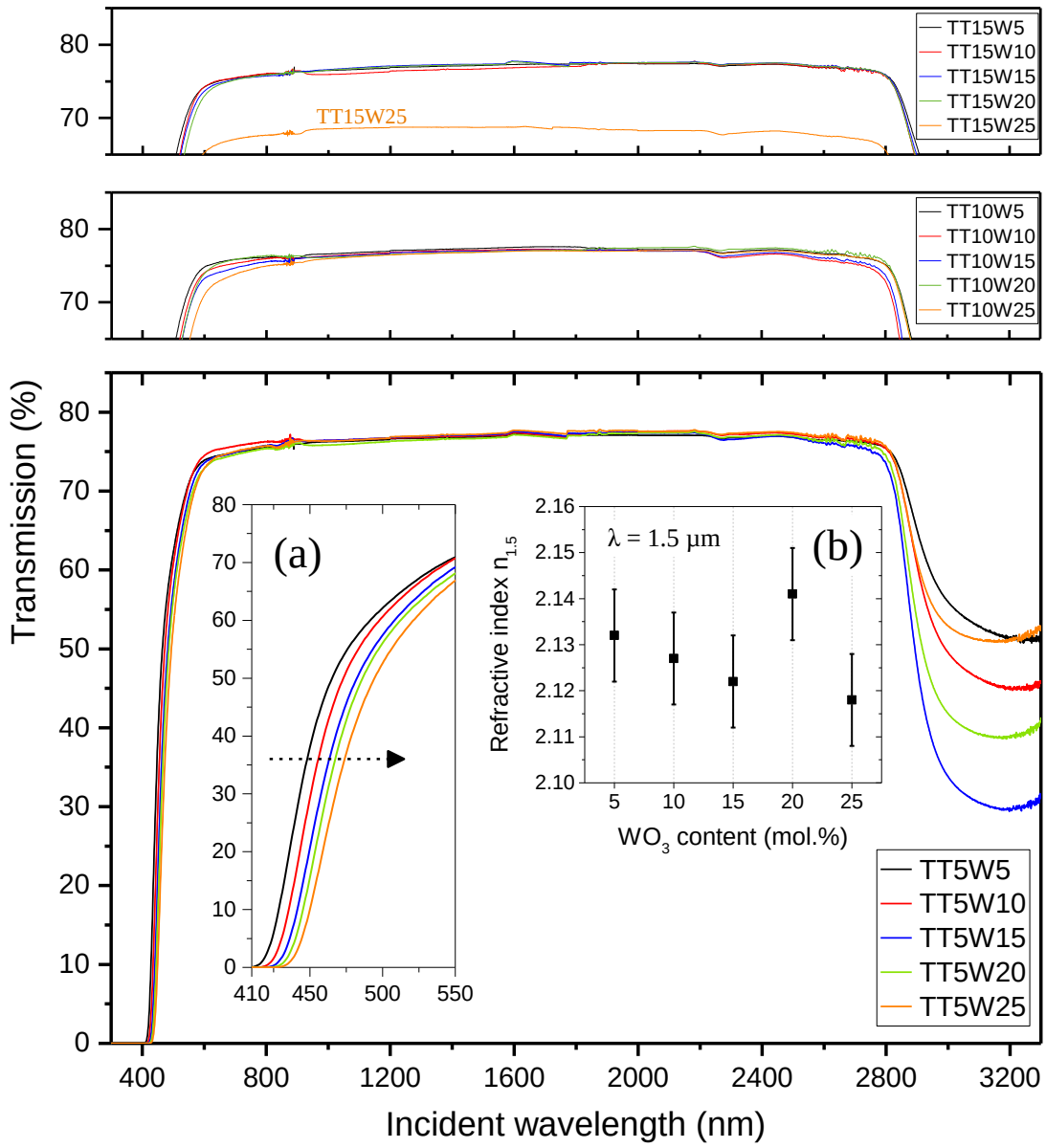
TT15W5
TT15W10
TT15W15
TT15W20
TT15W25
TT15W25
TT10W5
TT10W10
TT10W15
TT10W20
TT10W25
Transmission (%)
Incident wavelength (nm)
TT5W5
TT5W10
TT5W15
TT5W20
TT5W25
(a)
(b)
λ = 1.5 µm
Refractive index n1.5
WO3 content (mol.%)

Figure 9

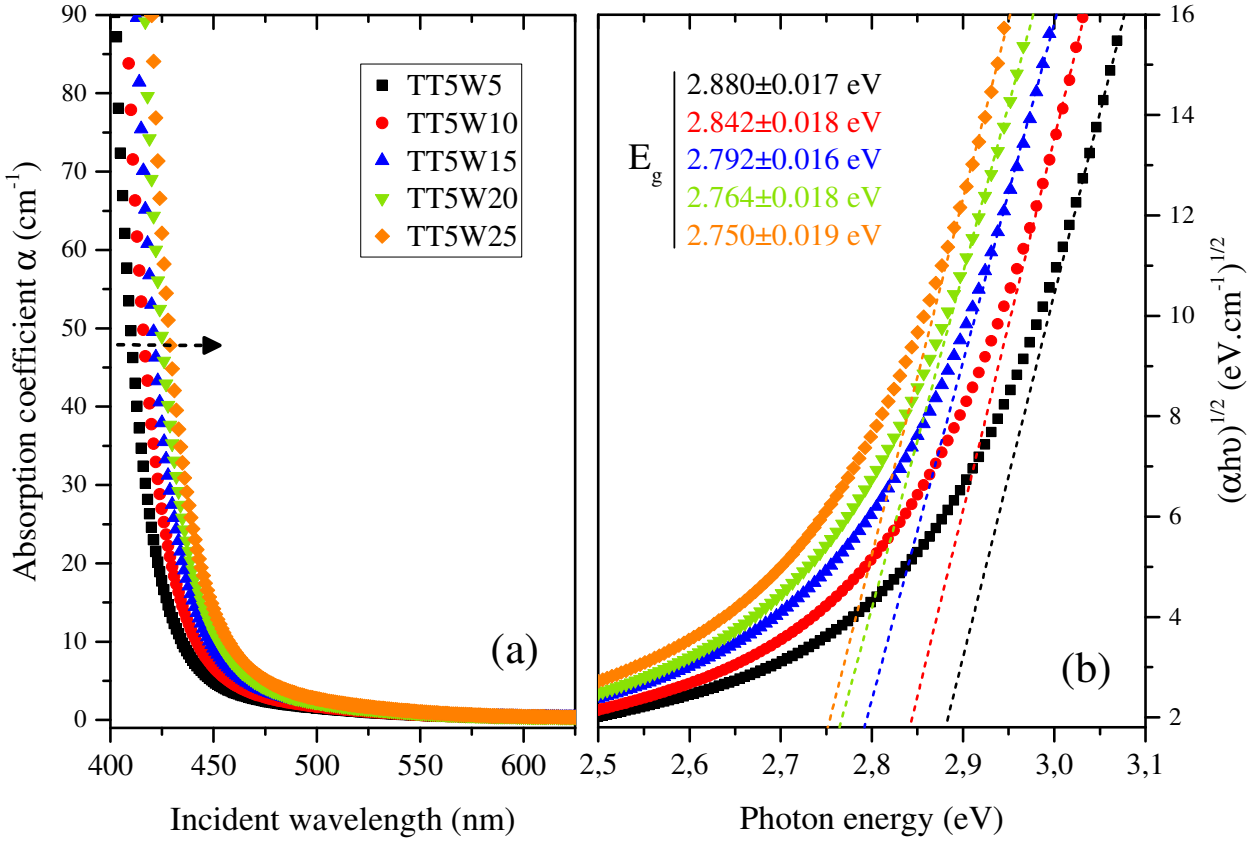
Absorption coefficient α (cm-1)
Incident wavelength (nm)
TT5W5
TT5W10
TT5W15
TT5W20
TT5W25
(a)
Eg
2.880±0.017 eV
2.842±0.018 eV
2.792±0.016 eV
2.764±0.018 eV
2.750±0.019 eV
(b)
Photon energy (eV)
(αhυ)1/2 (eV.cm-1)1/2

Figure 10

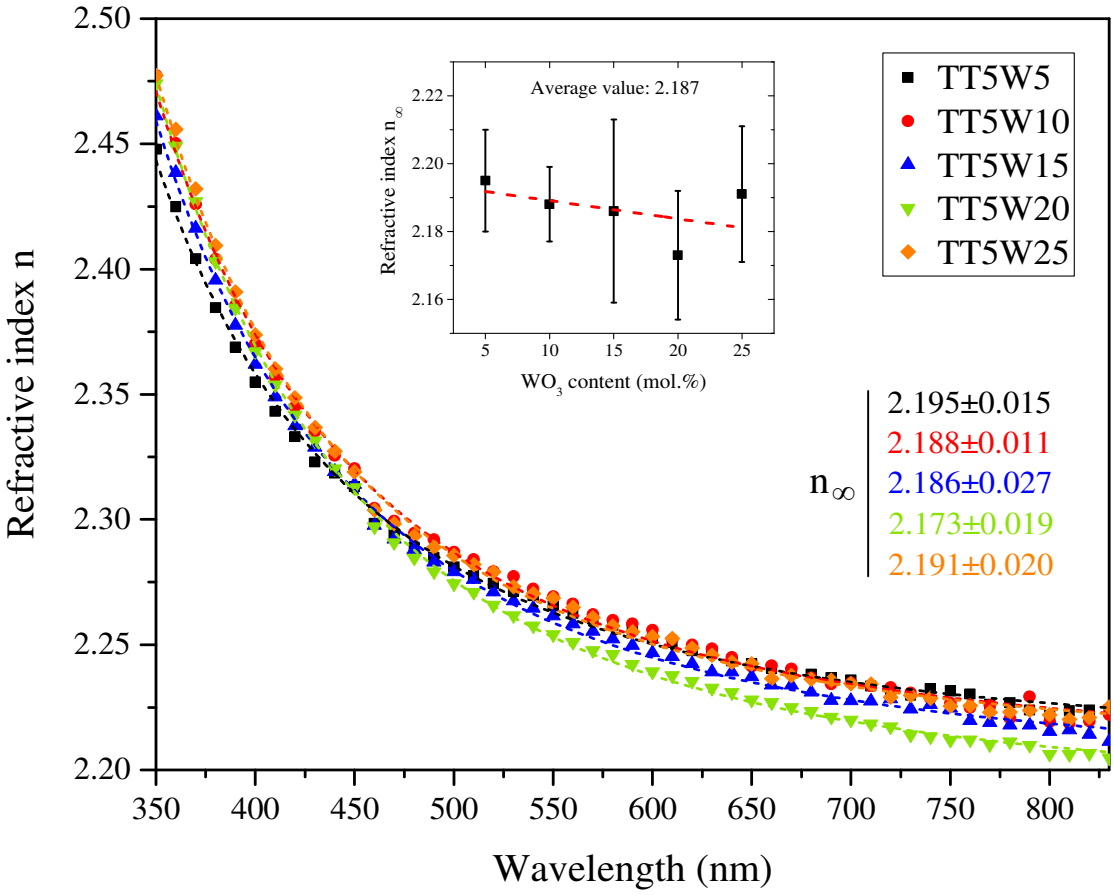
Refractive index n
Wavelength (nm)
2.50
2.45
2.40
2.35
2.30
2.25
2.20
350
400
450
500
550
600
650
700
750
800
TT5W5
TT5W10
TT5W15
TT5W20
TT5W25
n∞
2.195±0.015
2.188±0.011
2.186±0.027
2.173±0.019
2.191±0.020
Average value: 2.187
Refractive index n∞
WO3 content (mol.%)
2.22
2.20
2.18
2.16
5
10
15
20
25